

A Stringy Mechanism for A Small Cosmological Constant - Multi-Moduli Cases -

Yoske Sumitomo¹ and S.-H. Henry Tye^{1,2}

¹ Institute for Advanced Study, Hong Kong University of Science and Technology, Hong Kong

² Laboratory for Elementary-Particle Physics, Cornell University, Ithaca, NY 14853, USA

Email: yoske at ust.hk, iastye at ust.hk

Abstract

Based on the properties of probability distributions of functions of random variables, we proposed earlier a simple stringy mechanism that prefers the meta-stable vacua with a small cosmological constant Λ . As an illustration of this approach, we study in this paper particularly simple but non-trivial models of the Kähler uplift in the large volume flux compactification scenario in Type IIB string theory, where all parameters introduced in the model are treated either as fixed constants motivated by physics, or as random variables with some given probability distributions. We determine the value w_0 of the superpotential W_0 at the supersymmetric minima, and find that the resulting probability distribution $P(w_0)$ peaks at $w_0 = 0$; furthermore, this peaking behavior strengthens as the number of complex structure moduli increases. The resulting probability distribution $P(\Lambda)$ for meta-stable vacua also peaks as $\Lambda \rightarrow 0$, for both positive and negative Λ . This peaking/divergent behavior of $P(\Lambda)$ strengthens as the number of moduli increases. In some scenarios for $\Lambda > 0$, its expectation value $\langle \Lambda \rangle$ decreases as the number of moduli increases. The light cosmological moduli problem accompanying a very small Λ is also discussed.

Contents

1	Introduction	1
2	Background and Review	8
2.1	Probability distribution of functions of random variables	9
2.2	The single Kähler modulus model	10
3	Multiple complex structure moduli cases	13
3.1	Supersymmetric Minimum	14
3.2	Some properties of $w_0 = W_0 _{\min}$	16
3.3	Numerical comparison of w_0	17
3.4	Inserting the w_0 solution into the single Kähler modulus model	19
3.5	Some remarks	22
4	Multi-Kähler moduli cases	23
4.1	Uniformly distributed W_0, A_i	25
4.2	Sharply peaked $P(W_0)$ and uniform distribution $P(A_i)$	27
4.3	Sharply peaked $P(W_0)$ and $P(A_i)$	29
5	Discussions and Remarks	31
A	Some toy models	33
B	$P(\Lambda)$ in the single Kähler modulus case	35
C	Special symmetric case for s and w_0	36
D	Stabilization in two and three Kähler moduli models	37
D.1	Two Kähler moduli	37
D.2	Three Kähler moduli	39
D.3	Checking the validity of the approximate potential	39

1 Introduction

Recent cosmological data strongly suggests that our universe has an exponentially small positive cosmological constant $\Lambda \sim 10^{-122} M_P^4$ (see [1] and references therein). On the other hand, string theory has so many possible meta-stable vacuum solutions that it should have at least a solution with such a small Λ [2]. So it leaves open the question why nature picks a vacuum solution with

such a very small Λ , in units of the Planck scale. In a previous paper [3], we propose a plausible reason why this may happen within the context of string theory.

The basic idea is very simple. A typical compactification in string theory involves many moduli and fluxes (see the review [4]). The moduli and their dynamics describe the string theory landscape. Stabilizing them will lead to a set of values for these moduli, so Λ of a meta-stable vacuum will be a function of them. Many if not most of the moduli can take multiple (some discrete) values since each stabilized compactification involves a set of quantized fluxes. As a result, many of these moduli will take values within a range that include zero. If (and this is a big if) Λ is a product of some of them, then the probability distribution $P(\Lambda)$ of Λ will naturally peak (even mildly diverge) at $\Lambda = 0$. In actual models, the functional dependence of Λ on the parameters in the model is much more complicated. Here we show that the peaking property of $P(\Lambda)$ is present in the stringy scenarios studied here.

In [3], we work out the case for a single Kähler modulus in the Kähler uplifting region [5–8] of the Large Volume Scenario [9] in Type IIB string theory. There we treat the few parameters in the model as random variables and show that a modest suppression of Λ is achieved: despite of the non-trivial functional dependence of Λ on the parameters, $P(\Lambda)$ is peaked (actually diverges) at $\Lambda = 0$, even though the parameters are treated as random variables with uniform (or similarly smooth) distributions. In this single Kähler modulus model [3], we see that the suppression of Λ is present but very modest. In this paper, we consider the multi-moduli cases to check the validity of the basic idea. Here our probability and statistical analysis is largely based on the study by Rummel and Westphal [7] on a simplified yet non-trivial model in the Large Volume Scenario. Although the functional dependence of Λ on the parameters is more non-trivial, we still find that the probability distribution $P(\Lambda)$ for meta-stable vacua becomes more peaked at $\Lambda = 0$ (even mildly diverges) as the number of moduli increases. However, whether the expected value of Λ decreases exponentially or not as the number of moduli increases depends on the details of the physics which remains to be better understood.

To be more specific, consider a Swiss-cheese type of Calabi-Yau three-fold with $h^{1,1}$ number of Kähler moduli and $h^{2,1}$ number of complex structure moduli (so the manifold M has Euler number $\chi(M) = 2(h^{1,1} - h^{2,1})$ and we are mainly interested in negative $\chi(M)$). The simplified

model of interest is given by, setting $M_P = 1$,

$$\begin{aligned}
V &= e^K \left(K^{I\bar{J}} D_I W D_{\bar{J}} \bar{W} - 3 |W|^2 \right), \\
K &= K_K + K_d + K_{cs} = -2 \ln \left(\nu + \frac{\hat{\xi}}{2} \right) - \ln (S + \bar{S}) - \ln \left(-i \int \bar{\Omega} \wedge \Omega \right), \\
\mathcal{V} \equiv \frac{\text{vol}}{\alpha'^3} &= \gamma_1 (T_1 + \bar{T}_1)^{3/2} - \sum_{k=2}^{h^{1,1}} \gamma_k (T_k + \bar{T}_k)^{3/2}, \quad \hat{\xi} = -\frac{\zeta(3)}{4\sqrt{2}(2\pi)^3} \chi(M) (S + \bar{S})^{3/2}, \\
W &= W_0(U_i, S) + \sum_{k=1}^{h^{1,1}} A_k e^{-a_k T_k},
\end{aligned} \tag{1.1}$$

where Ω is the homomorphic three-form. In the superpotential W , the flux contribution to $W_0(U_i, S)$ depends on the dilation S and the $h^{2,1}$ complex structure moduli U_i ($i = 1, 2, \dots, h^{2,1}$), while the non-perturbative terms for $h^{1,1}$ Kähler moduli T_k ($k = 1, 2, \dots, h^{1,1}$) are introduced in W [10]. The dependence of A_i on U_i, S are suppressed. The model also includes the α' -correction (the $\hat{\xi}$ term) to the Kähler potential [11]. This model was originally proposed for the Large Volume Scenario [9] (see also [12–14]), and has been further analyzed in the search of de-Sitter vacua [5–8].

Since we like to study the behavior of the expectation value of Λ when the number of complex structure moduli fields is large, we employ a simple model motivated by the orientifolded orbifolds of T^6 [7, 15], given by

$$\begin{aligned}
K_{d+cs} &= -\ln (S + \bar{S}) - \sum_{i=1}^{h^{2,1}} \ln (U_i + \bar{U}_i), \\
W_0(U_i, S) &= c_1 + \sum_{i=1}^{h^{2,1}} b_i U_i - S \left(c_2 + \sum_{i=1}^{h^{2,1}} d_i U_i \right),
\end{aligned} \tag{1.2}$$

where c_i, b_i and d_i are (real) flux parameters that may be treated as random variables with smooth probability distributions that allow the zero values. Here we are interested in the physical Λ (instead of, say, the bare Λ), so the model should include all appropriate non-perturbative effects, α' corrections as well as radiative corrections. We see that the above simplified model (1.1) includes non-perturbative A_k terms to stabilize the Kähler moduli and the α' correction $\hat{\xi}$ term to lift the solution to de-Sitter space. In the same spirit, all parameters in the model, in particular the coupling parameters c_i, b_i and d_i in W_0 (1.2), should be treated as physical parameters that have included all relevant corrections.

Following the analysis of [16–20], we expect that the probability of an extremum at positive vacuum energy to be a classically stable solution will be Gaussianly suppressed (see also an estimation at supersymmetric AdS in SUGRA [21]). So the existence of solutions will put constraints on the parameters and we take $s = \text{Re}(S) = 1/g_s > 1$ for weak coupling. It

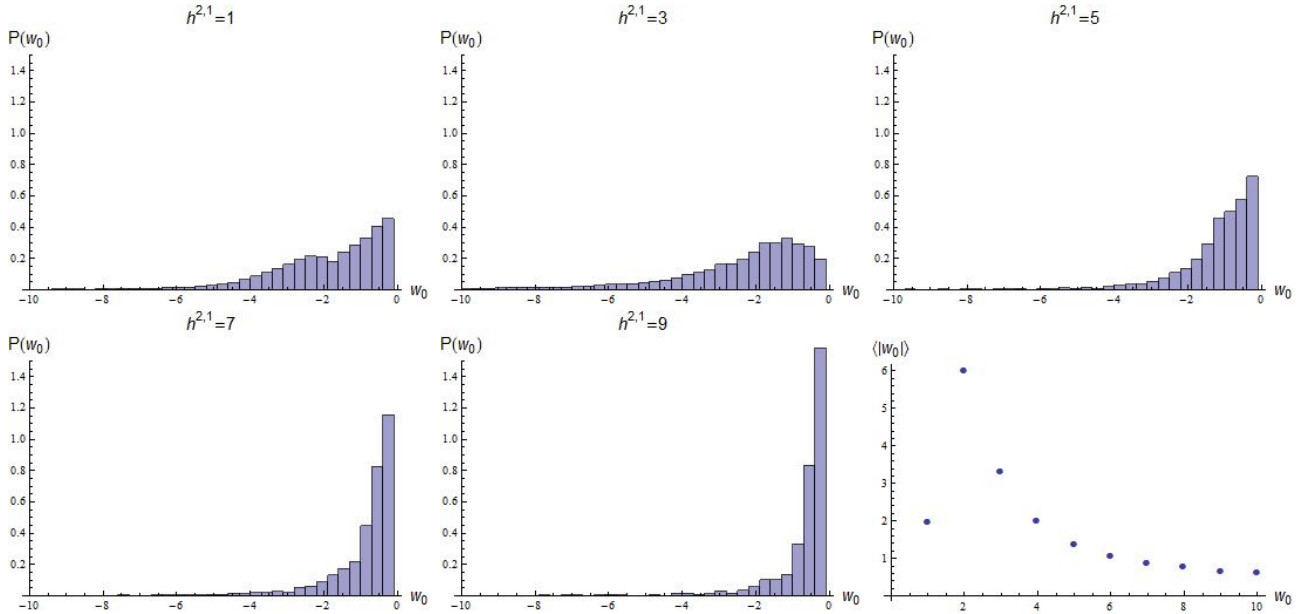


Figure 1: The probability distribution $P(w_0)$ for w_0 (1.3) with $h^{2,1} = 1, 3, 5, 7, 9$ number of complex structure moduli respectively, where w_0 is the value of the superpotential W_0 at the supersymmetric solution. Here we present $P(w_0)$ in the range $-10 \leq w_0 \leq 0$ ($\int_{-10}^0 P(w_0) dw_0 = 1$) after solving for the complex structure moduli and the dilation at the supersymmetric point satisfying $s > 1$ for weak string coupling and $u_i > 0$ for the Kähler potential to be real. After some transient behaviors at small $h^{2,1}$, the peaking (at $w_0 = 0$) of $P(w_0)$ strengthens as $h^{2,1}$ increases. In the last figure, we show the behavior of the expectation value $\langle |w_0| \rangle$.

turns out to be a good approximation to stabilize the U_i and S at a supersymmetric minimum ($D_S W_0 = D_{U_i} W_0 = 0$) before turning on the corrections for the stabilization of the Kähler moduli, which then breaks supersymmetry. At the supersymmetric minimum with their axionic components sitting at zero, $u_i = \text{Re}(U_i) > 0$ (required for $K_{\text{d+cs}}$ (1.2) to stay real) and $s > 1$ are determined and

$$w_0 \equiv W_0|_{\min} = -\frac{2(c_1 + sc_2)\prod_{i=1}^{h^{2,1}}(1 - sr_i)}{\sum_{i=1}^{h^{2,1}}(1 + sr_i)\prod_{j \neq i}(1 - sr_j)}, \quad (1.3)$$

where $r_i = d_i/b_i$ and s is given as a function of the real random parameters c_1, c_2, r_i .

In general, the parameters will be fixed constants within the supergravity framework. However, it is the flux compactification property in string theory that allows us to compare solutions with different choices of values for the parameters (e.g., different choices of fluxes may stabilize the complex structure moduli and dilaton differently). So we are justified to treat the parameters as variables with some suitable probability distributions and study the consequences. In this sense, the mechanism we suggest here can be considered as a stringy mechanism. As we sweep through the (e.g., uniform) distributions for the parameters c_1, c_2, b_i, d_i , we see that each factor in the numerator of (1.3) easily passes through zero. So we expect the probability distribution $P(w_0)$ of the value for the superpotential $w_0 = W_0|_{\min}$ to become more peaked at $w_0 \rightarrow 0$ as the number $h^{2,1}$ of complex structure moduli increases (e.g., to hundreds). This behavior is

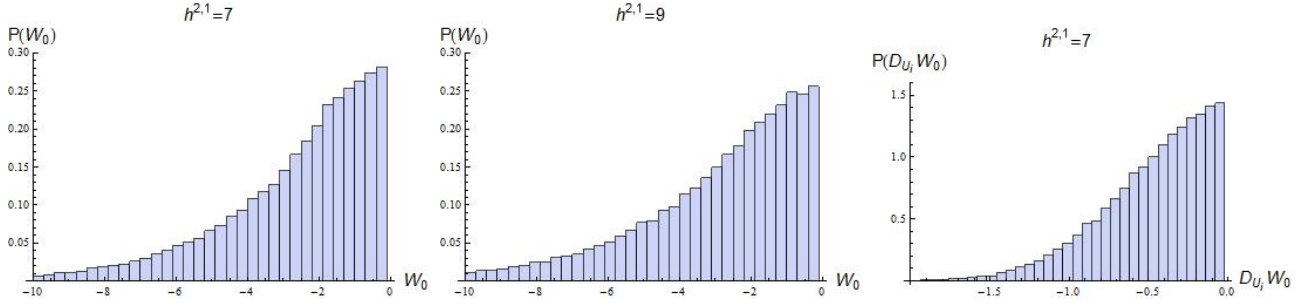


Figure 2: The probability distribution $P(W_0)$ of W_0 (1.2) when the real components of the dilation and the complex structure moduli are also treated as random variables. Here we assume uniform distributions with ranges $-1 \leq c_i, b_i, d_i \leq 1$, $1 < s \leq 5$, and $0 < u_i \leq 1$. The first 2 figures are for $P(W_0)$ for $h^{2,1} = 7, 9$. The third figure is for $P(D_{U_i} W_0)$ of $D_{U_i} W_0$ for $h^{2,1} = 7$.

illustrated in Figure 1.

It is interesting to compare $P(w_0)$ of w_0 (1.3) after stabilization with the probability distribution $P(W_0)$ of W_0 (1.2) before stabilization. Let us choose the same uniform distributions for c_i, b_i, d_i used in Figure 1, but instead of solving for u_i and s , we treat them as random variables with uniform distributions with range $0 \leq u_i \leq 1$ and $1 < s \leq 5$ (while the axionic modes are suppressed). With these uniform distributions, we show $P(W_0)$ in Figure 2; it is clearly smooth at $W_0 = 0$. We note that the probability distributions $P(D_{U_i} W_0)$ for the variables $D_{U_i} W_0$ are also smooth with little or no preference for the zero value, as expected. If $P(W_0)$ and $P(D_{U_i} W_0)$ are truly independent distributions, then fixing $D_{U_i} W_0 = 0$ (and $D_S W_0 = 0$) will not change the distribution $P(W_0)$; that is, $P(w_0)$ should be the same as $P(W_0)$. However, this is clearly not the case when we compare Figure 1 (for $P(w_0)$) and Figure 2 (for $P(W_0)$). This is because the two “random” distributions $P(W_0)$ and $P(D_{U_i} W_0)$ are actually correlated. In general, given any specific model, we expect correlations between these two distributions (as well as those for DDW_0 and $DDDW_0$). It is this correlation that leads to the peaking feature in $P(w_0)$ in Figure 1.

Next we insert the value w_0 into the superpotential W which is then inserted into the potential V . This allows us to find Λ for the de-Sitter meta-stable vacua via the stabilization of the Kähler moduli. This hierarchical setup effectively reduces the number of moduli fields when we reach the energy level for the Kähler moduli stabilization with determined s and the complex structure moduli u_i , and thus helps to enhance the probability for dS vacua. Since the SUGRA approximation is valid only if the scale of the potential V is around or below the Planck scale, we have to restrict ourselves to such a valid set of potentials V in the determination of Λ . Among these meta-stable vacua, we expect that the probability distribution $P(\Lambda)$ for Λ will also peak at $\Lambda = 0$. The numerical result on $P(\Lambda)$ for the single Kähler modulus scenario is shown in Figure 3.

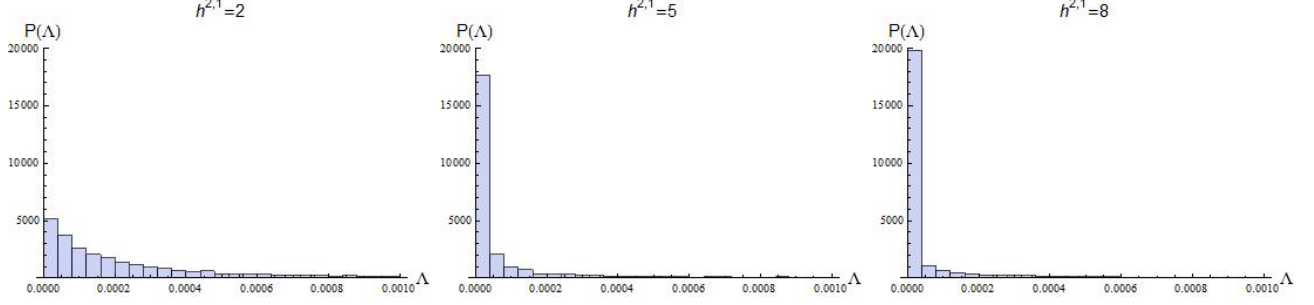


Figure 3: The probability distribution $P(\Lambda)$ of the cosmological constant Λ at meta-stable vacua as a function of $h^{2,1} = 2, 5, 8$ number of complex structure moduli and a single Kähler modulus ($h^{1,1} = 1$). Although the range is $0 \leq \Lambda \lesssim 1$, the probability distributions for only $0 \leq \Lambda \leq 10^{-3}$ are shown. $P(\Lambda)$ becomes more peaked at $\Lambda = 0$ as $h^{2,1}$ increases.

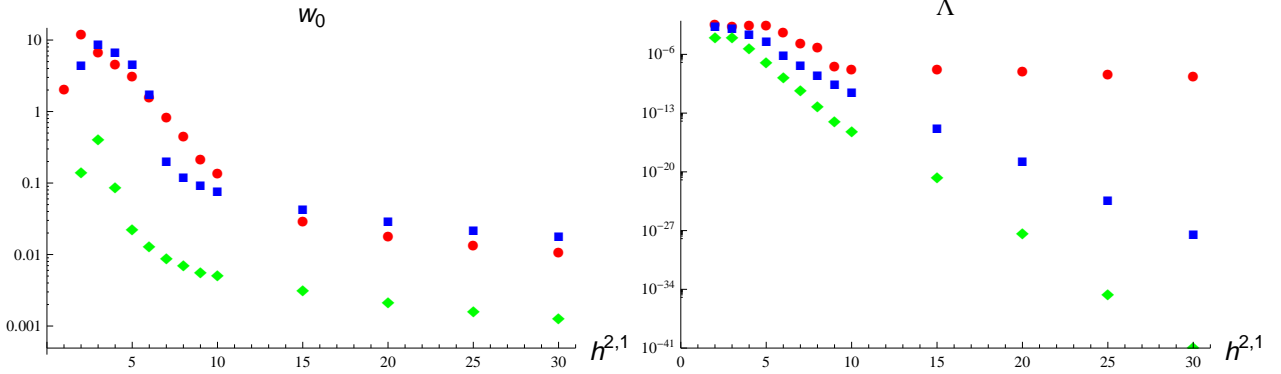


Figure 4: The LHS shows the average $\langle |w_0| \rangle$ (red circles), $|w_0|^{80\%}$ (blue squares) and $|w_0|^{10\%}$ (green diamonds) as a function of the number $h^{2,1}$ of complex structure moduli. The RHS shows $\langle \Lambda \rangle$ (red circles), $\Lambda^{80\%}$ (blue squares) and $\Lambda^{10\%}$ (green diamonds) as a function of $h^{2,1}$. That is, there is a $Y\%$ probability that Λ of the meta-stable vacua will fall in the range $\Lambda^{Y\%} \geq \Lambda \geq 0$. For example, $\Lambda^{10\%} \simeq 4.8 \times 10^{-28}$ at $h^{2,1} = 20$ and $\simeq 1.5 \times 10^{-41}$ at $h^{2,1} = 30$ (green diamonds). The values are for the case where the b_i parameters are fixed.

Although the peaking property of $P(\Lambda)$ is essential for the preference of a very small Λ , it is not enough. We find that the expectation value $\langle \Lambda \rangle$ for de-Sitter vacua more or less stays constant (or changes little) as the number of complex structure moduli increases. That is, $P(\Lambda)$ in this scenario has a long tail outside the $\Lambda \sim 0$ region.

However, there are more than one way to implement the distributions for the random parameters. Since $u_i = w_0/2b_i(1 - sr_i)$, allowing $b_i = 0$ implies that we are looking at vacua where some $u_i \rightarrow \infty$, which may not be valid within our approximation. So, as an alternative, let us restrict the values of b_i to a range that excludes zero, say $0 > -f_{min} \geq b_i \geq -f_{max}$. It turns out that the qualitative physics does not change if we simply restrict b_i to a fixed value, say $b_i = -f < 0$, where we may consider $-f$ to be the mid-point of the range for b_i . We shall choose f so that 90% of the resulting Λ falls in the range $1 \gtrsim \Lambda \geq 0$, which we keep (our analysis is

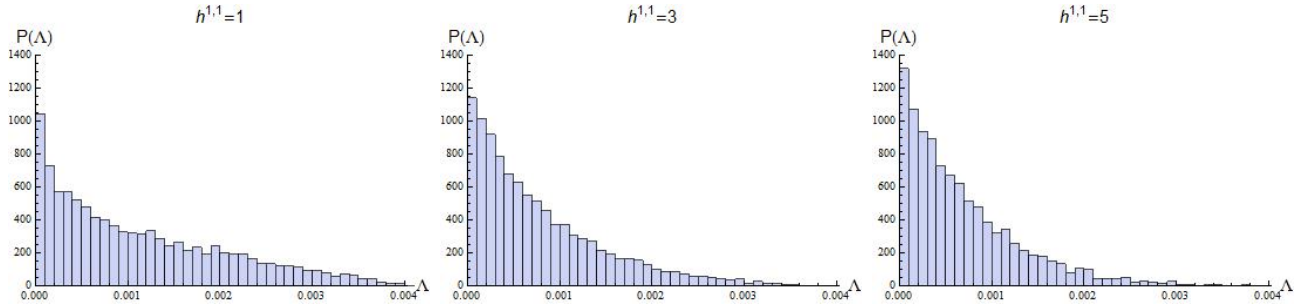


Figure 5: The probability distribution $P(\Lambda)$ for the $h^{1,1} = 1, 3, 5$ Kähler moduli cases with uniformly distributed W_0, A_i . Note that $P(\Lambda = 0)$ is increasing (slowly) as $h^{1,1}$ increases.

probably not valid for larger Λ). In this scenario, both $P(w_0)$ and $P(\Lambda)$ are peaked at zero, not too different from Figures 1 and 3; while, for $\Lambda \geq 0$, $\langle \Lambda \rangle \sim e^{-2.56 h^{2,1} + 7.40}$ for $h^{2,1} \leq 10$. However, the drop of $\langle \Lambda \rangle$ slows down appreciably as $h^{2,1} > 10$ (see Figure 4). These examples show that the behavior of $\langle \Lambda \rangle$ is very sensitive to the details of the input distributions of the parameters. On the other hand, the peaking (divergent or not) behavior of $P(\Lambda)$ as $\Lambda \rightarrow 0$ is quite robust.

To get a better feeling of the peaking property of $P(\Lambda)$ for $\Lambda \geq 0$, let us introduce $\Lambda^{Y\%}$, defined by $\int_0^{\Lambda^{Y\%}} P(\Lambda) d\Lambda = Y\%$. That is, there is a $Y\%$ probability that Λ of the meta-stable vacua will fall in the range $\Lambda^{Y\%} \geq \Lambda \geq 0$. (Note that $\Lambda^{100\%} \simeq 1$.) In Figure 4, we show $\langle \Lambda \rangle$, $\Lambda^{80\%}$ and $\Lambda^{10\%}$ as a function of the number of complex structure moduli. For example, at $h^{2,1} = 20$, while $\langle \Lambda \rangle \simeq 1.2 \times 10^{-8}$, $\Lambda^{80\%} \simeq 2.0 \times 10^{-19}$ and $\Lambda^{10\%} \simeq 4.8 \times 10^{-28}$. For $h^{2,1} = 30$, we find that $\Lambda^{10\%} \simeq 1.5 \times 10^{-41}$; that is, there is a 10% chance that $\Lambda \lesssim 1.5 \times 10^{-41}$ in this case. If we take a cutoff lower than the 90% used, the resulting Λ values will be bigger (i.e., less impressive). For comparison, we also show in Figure 4 the average $\langle w_0 \rangle$ and the corresponding $w_0^{80\%}$ and $w_0^{10\%}$.

We also consider the multi-Kähler moduli cases. In Figure 5, we show $P(\Lambda)$ for $h^{1,1} = 1, 2, 3$ Kähler moduli cases (where the complex structure moduli and dilation are suppressed). We see that the peaking behavior also strengthens as the number of Kähler moduli increases. For positive Λ , we have $\langle \Lambda \rangle \sim 0.00110 (h^{1,1})^{-0.226} e^{-0.0268 h^{1,1}}$, where uniformly distributed W_0, A_i are assumed. Here, the coefficient in the exponent is actually too small to be taken seriously. However, if we have sharply peaked distributions in W_0 and A_i , a clear exponential suppression in $\langle \Lambda \rangle$ as a function of $h^{1,1}$ is expected. We shall illustrate these features with some simplified models.

In short, we see that $P(\Lambda)$ becomes more peaked at $\Lambda = 0$ as the number of moduli increases. This feature is robust. On the other hand, the behavior of $\langle \Lambda \rangle$ (or $\sqrt{\langle \Lambda^2 \rangle}$) is sensitive to the way we implement the random parameter distributions and other inputs. The model studied here is chosen for its simplicity. The numerical data presented here are for the specific scenarios described. There may be other interesting scenarios within this simple model. To go beyond, it is important to examine more realistic models to check (1) whether the peaking of $P(\Lambda)$ at

$\Lambda = 0$ is as robust as we believe, and (2) what models will lead to an exponentially decreasing $\langle |\Lambda| \rangle$ (or $\Lambda^{Y\%}$) as a function of the number of moduli. A better understanding of the underlying physics should allow us to determine the value of $\langle |\Lambda| \rangle$ or $\Lambda^{Y\%}$ as a function of the number of moduli. An exponentially decreasing $\langle |\Lambda| \rangle$ or $\Lambda^{Y\%}$ may be used as a criteria to select particular regions of the landscape.

In general, the probability that an extremum happens to be a meta-stable vacuum is Gaussianly unlikely as the number of moduli increases, as discussed in [16–21]. It is our goal to find scenarios where an exponentially small Λ for a meta-stable vacuum is preferred when the number of complex structure moduli is large, as one expects to be the case in any realistic model. In fact, some of the commonly studied Calabi-Yau 3-folds with one Kähler modulus are smooth hypersurfaces in \mathbb{CP}^4 with hundreds of complex structure moduli. So an exponentially small Λ hopefully may be naturally realized in this framework.

Note that having a very small Λ does not necessarily solve the Λ problem completely. In this setup, the expectation value of the mass (squared) of the lightest modulus tends to decrease more quickly than $\langle \Lambda \rangle$. So we may have the cosmological moduli problem [22–24]. It remains to be seen whether the light modulus mass is really a phenomenological problem as one may intuitively envision.

In summary, we find that the study of multi-moduli scenarios is a promising direction in the search for the reason why the observed Λ is so small. Tremendous amounts of effort have been spent on the search for a string vacuum with a standard model of three families of quarks and leptons. We believe it is worthwhile to search for regions of vacua in the stringy cosmic landscape that have a chance of providing a naturally small positive Λ . Combining these two criteria in a search may be more effective than the searches carried out so far. On a separate note, we hope that this product distribution idea can find applications in other phenomena.

The rest of the paper is organized as follows. Section 2 reviews some simple probabilistic properties of functions of random variables and the single Kähler modulus model. Section 3 discusses the multi-complex structure moduli case. Here we find the supersymmetric solutions for the complex structure moduli and the dilation and then insert them into the single Kähler modulus model to solve for Λ . Section 4 discusses the multi- Kähler cases. Here, we also consider some simplified versions of the general multi-moduli cases. Section 5 presents the summary and discussions. Some details are relegated to the appendices.

2 Background and Review

We begin with a review of the basic probability distribution of a function of random variables when the distributions of the random variables are given. In particular, we emphasize on the

peaking property in the resulting probability distribution, since this is relatively insensitive to the details. We explain how a product of random variables gets a sharply peaked (at zero) probability distribution. We also point out the importance of the overall distributions to the expectation values. Then we review how this feature emerges for the probability distribution of Λ in the single Kähler modulus model in a class of models in Type IIB string theory well studied already, basically following [3]. We shall use this model to provide the framework to study the multiple complex structure moduli scenarios. In appendix A, we give some field theory toy models to illustrate some of the probabilistic properties that one may encounter in this analysis.

2.1 Probability distribution of functions of random variables

Suppose we have n random variables y_i ($i = 1, 2, \dots, n$), each with probability distribution $P_i(y_i)$, where $\int P_i(y_i) dy_i = 1$. Let us consider an arbitrary function $z = f(y_1, y_2, \dots, y_n)$. Then the probability distribution $P(z)$ of z is given by

$$P(z) = \int dy_1 dy_2 \cdots dy_n P_1(y_1) P_2(y_2) \cdots P_n(y_n) \delta(f(y_i) - z),$$

$$\int P(z) dz = 1,$$
(2.1)

so the probability distribution $P(z)$ of z can always be properly normalized, even when $P(z)$ diverges at $z = 0$ and/or elsewhere.

Consider the following simple example: $z = y_1 y_2 \cdots y_n$ and each random parameter y_i obeys the uniform distribution $P(y_i) = 1/L$ with range $0 \leq y_i \leq L$; then the probability distribution $P(z)$ of z is given by (for $0 \leq z \leq L^n$)

$$P(z) = \int_0^L \frac{dy_1}{L} \frac{dy_2}{L} \cdots \frac{dy_n}{L} \delta(y_1 y_2 \cdots y_n - z) = \frac{1}{(n-1)! L^n} \left(\ln \frac{L^n}{|z|} \right)^{n-1}. \quad (2.2)$$

Therefore $P(z)$ of a product of random parameters has a mild divergent peak at $z = 0$. This divergent behavior strengthens as n increases. Actually this logarithmic divergent behavior of $P(z)$ at $z = 0$ (2.2) is present for any y_i distribution that smoothly includes $y_i = 0$.

Given the probability distribution for y_i , we can determine its expectation value. Here, for $z = y_1 y_2 \cdots y_n$, the expectation value of the p th moment $\langle z^p \rangle$ of z is given by

$$\langle z^p \rangle = \langle y_1^p \rangle \cdots \langle y_n^p \rangle \quad (2.3)$$

following from the property of Mellin integral transformation. Since $\langle y_i \rangle = L/2$ for the uniform distribution, we have

$$\langle z \rangle = \left(\frac{L}{2} \right)^n = e^{-n \ln(2/L)}. \quad (2.4)$$

For $L < 2$, we see that $\langle z \rangle$ decreases exponentially as n increases; so the divergent behavior at $z = 0$ is correlated to the smallness of $\langle z \rangle$. However, $\langle z \rangle$ increases exponentially if $L > 2$. In this case, the long tail (at large z) of $P(z)$ drives $\langle z \rangle$. In short, we see that the behavior of $\langle z \rangle$ (as a function of n) is very sensitive to the property of $P(z)$, especially at large z .

To conclude, we like to mention that $P(z)$ is in general smooth at $z = 0$ if z is a sum of terms that involve independent random variables (see e.g. [3] for more details). The problem now is to find the functional form of the cosmological constant Λ of meta-stable vacua in terms of the random parameters entering the model and see whether its distribution has the nice peaking property at zero and whether its expectation value or $\Lambda^{Y\%}$ decreases exponentially fast as a function of the number of moduli.

2.2 The single Kähler modulus model

We briefly review the analytic study of the probability distribution $P(\Lambda)$ in the single Kähler modulus scenario in type IIB string theory [3]. Although no potential is generated for the Kähler modulus at the classical tree level, non-perturbative terms can be introduced into the superpotential W and α' -corrections into the Kähler potential to break the no-scale structure, so that a non-trivial potential is generated at next leading order. The tree level potential basically controls the stabilization of complex structure moduli and dilaton. Here we simply assume the complex structure sector is stabilized at high-energy levels and therefore is believed to have been integrated out in the low energy effective model. Later, we shall introduce the complex structure sector, solve it at the supersymmetric point and insert the solution into this model to solve for the stabilization of the Kähler modulus which then breaks supersymmetry.

The model of interest is given in [5–8], also known as *Kähler uplifting model* :

$$\begin{aligned} K &= -2 \ln \left(\mathcal{V} + \frac{\hat{\xi}}{2} \right), \quad \mathcal{V} = \gamma_1 (T_1 + \bar{T}_1)^{3/2}, \\ W &= W_0 + A_1 e^{-a_1 T_1}, \end{aligned} \tag{2.5}$$

where the α' -correction related to the $\hat{\xi}$ term [11] and non-perturbative correction with the parameter A_1 [10] are given. The parameters W_0, A_1 will be treated as random variables. We work within the approximation

$$\frac{\hat{\xi}}{\mathcal{V}} \ll 1, \quad \left| \frac{A_1 e^{-a_1 T_1}}{W_0} \right| \ll 1, \tag{2.6}$$

to simplify the analytical study [7]. We shall see that this approximation is quite reasonable for the analysis of small Λ . The first approximation is a sort of the large volume approximation which is powerful for suppressing the other unwanted stringy corrections.

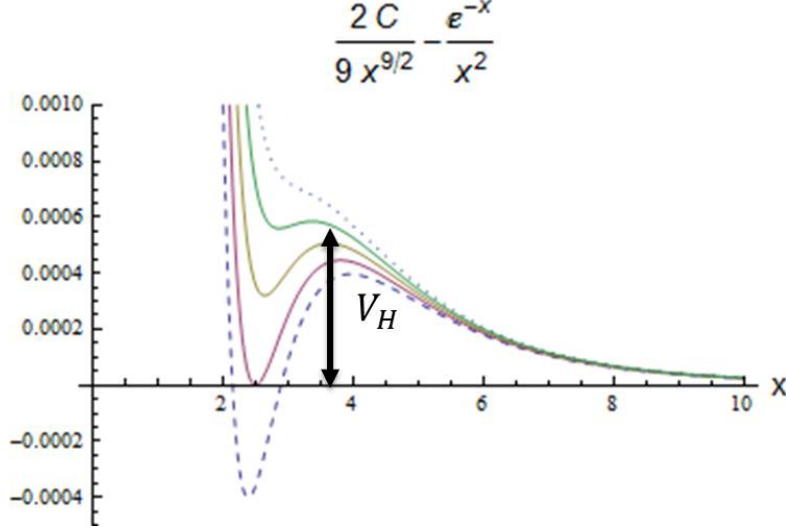


Figure 6: The potential V for different values of C . Only the bracket part in V (2.7) is shown. The V_H defined at $C \sim 3.89$ gives roughly the height of the potential barrier.

Since the imaginary part of the Kähler modulus T_1 has a cosine type of potential, the extremal condition for this direction is satisfied when $\text{Im } T_1 = 0$. Therefore we focus only on real part $t_1 \equiv \text{Re } T_1$.

Now the potential simplifies to [7]

$$V \sim \frac{-W_0 a_1^3 A_1}{2\gamma_1^2} \left(\frac{2C}{9x_1^{9/2}} - \frac{e^{-x_1}}{x_1^2} \right), \quad (2.7)$$

$$C = \frac{-27W_0 \hat{\xi} a_1^{3/2}}{64\sqrt{2}\gamma_1 A_1}, \quad x_1 = a_1 t_1.$$

The stability condition $\partial_{x_1}^2 V > 0$ at the extrema $\partial_{x_1} V = 0$ with respect to x_1 is easy to analyze, and we get the parameter range for stable positive Λ :

$$C_0 \lesssim C < C_1 \quad \rightarrow \quad 3.65 \lesssim C < 3.89, \quad (2.8)$$

where the lower bound is given by positivity of the minimum of V , while the upper bound is given by the stability constraint. If we satisfy the combination of parameters C inside this region, there is a stable solution in the range $2.50 \lesssim x_1 < 3.11$ at $\Lambda \geq 0$. Up to an overall factor, the potential V (2.7) is shown in Figure 6.

Our interest is to study the statistical property at small Λ . In this approximation, the extremal condition gives us the linear relation between x_1 and C by

$$x_1 \sim \left(\frac{5}{2} \right)^{-5/2} e^{5/2} C - 2. \quad (2.9)$$

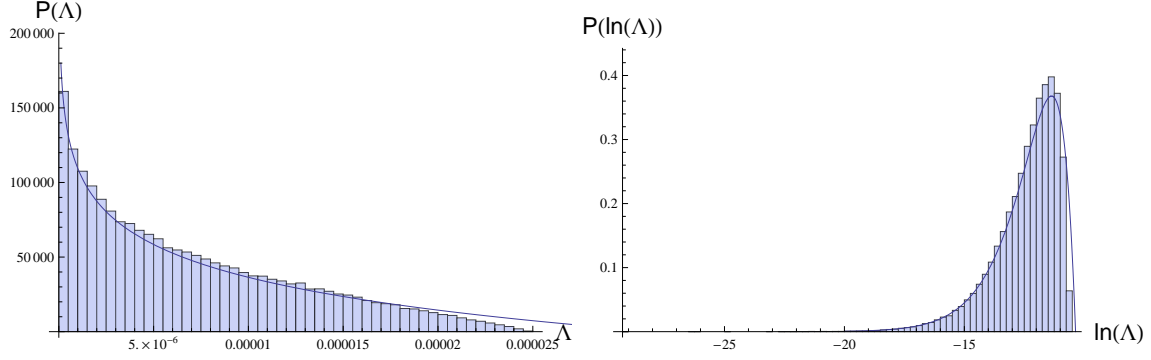


Figure 7: The comparison between the analytic result (2.12) (solid line) and the numerical result of the potential (2.5) (histogram). Here we set $a_1 = \gamma_1 = \xi = 1$ and assume uniform distribution for parameters W_0, A_1 . The plot in LHS shows the probability distribution $P(\Lambda)$ of Λ , while the plot in RHS is the probability distribution $P(\ln \Lambda)$ vs $\ln \Lambda$. They are related via $P(\Lambda) d\Lambda = P(\ln \Lambda) d\ln \Lambda$.

and we have

$$\Lambda \equiv V|_{\min} \sim \frac{1}{9} \left(\frac{2}{5} \right)^{9/2} \frac{-W_0 a_1^3 A_1}{\gamma_1^2} (C - 3.65). \quad (2.10)$$

Looking at V (2.10), we note that the height of the potential barrier is relatively unchanged as Λ varies from negative values to positive values, as shown in Figure 6. So we may use the barrier height as a measure of the scale of the potential V ,

$$V_H = \frac{1}{9} \left(\frac{2}{5} \right)^{9/2} \frac{-W_0 a_1^3 A_1}{\gamma_1^2} (0.24). \quad (2.11)$$

In general, the SUGRA approximation is valid if the scale of V is less than the Planck (or string) scale. We shall require $V_H \leq 1$ as the condition for the validity of our approximation.

In finding the probability distribution $P(\Lambda)$, the peaking behavior of the distribution comes essentially from this V_H . Since we would like to focus on the shape of distribution, we set the maximal value to be $V_H|_{\max} = 1$ here, such that the effective theory is safely applicable under the Planck scale. For further simplification, we may set $a_1, \gamma_1, \hat{\xi}$ to constants and see the effect of two random variables W_0, A_1 on $P(\Lambda)$. (In [3], we also discuss cases where the other parameters are treated as random variables.)

If we simply assume $0 \leq -W_0, A_1 \leq 1$ obeying uniform distribution, the probability distribution can be obtained (the detail is relegated to appendix B),

$$P(\Lambda) = \frac{2500\sqrt{5}}{3\delta C} \ln \left[\frac{3}{2500\sqrt{5}} \frac{\delta C}{\Lambda} \right]. \quad (2.12)$$

where $\delta C = (C_1 - C_0)/C_1 = 0.0617$. So we clearly see the divergent behavior as $\Lambda \rightarrow 0$. The stabilization dynamics is responsible for the divergent behavior in $P(\Lambda)$. As we state in

the introduction, the peaking behavior of $P(\Lambda)$ is robust. Note that this divergent behavior is present for negative Λ as well. For $\Lambda < 0$, there is another branch of supersymmetric AdS solutions; so $P(\Lambda)$ for $\Lambda < 0$ is not a reflection of the $P(\Lambda)$ shown above.

Let us compare $P(\Lambda)$ obtained analytically in the approximate potential (2.10) with that obtained numerically for the potential (2.5), as shown in Figure 7. From the two figures there, we see their nice agreement with each other, especially at small Λ .

3 Multiple complex structure moduli cases

So far we have reviewed the case with a single Kähler modulus assuming moduli stabilization of the complex structure and the dilaton at higher energy scale. In the actual models, we have the dilaton S and many complex structure moduli U_i ($i = 1, 2, \dots, h^{2,1} = N_{\text{cs}}$) which are assumed to be stabilized at a higher scale with fluxes as sources. Here, we analyze in more detail their stabilization and see how it affects the probability distribution of W_0 . In [25], a random distribution for the superpotential (and its derivatives) is assumed to investigate the entire landscape of SUGRA. Here, we probe parts of the SUGRA landscape in greater details.

Throughout this section, we focus on models of the form:

$$\begin{aligned} K_{\text{cs+d}} &= -\ln(S + \bar{S}) - \sum_{i=1}^{h^{2,1}} \ln(U_i + \bar{U}_i), \\ W_0 &= c_1 + \sum_{i=1}^{h^{2,1}} b_i U_i - \left(c_2 + \sum_{i=1}^{h^{2,1}} d_i U_i \right) S, \end{aligned} \tag{3.1}$$

where c_i, b_i, d_i are parameters from fluxes. This model is motivated by the orientifolded orbifolds of T^6 [7, 15], and is used for the purpose to see the tendency of the probability distribution of W_0 as a function of $h^{2,1}$ here. Supersymmetry breaking comes from the interplay between the α' correction $\hat{\xi}$ term and the non-perturbative term reviewed in section 2.2. So it is a good approximation to solve for U_i and S at the supersymmetric point and then insert their values into the full system to solve for the stabilization of the Kähler moduli. It is worth noting that we basically require $\hat{\xi} > 0$ (1.1) for the stability analyses of Kähler moduli later, meaning that the number of complex structure moduli is greater than the number of Kähler moduli: $\chi(M) = 2(h^{1,1} - h^{2,1}) < 0$. As pointed out in [7], this approximation is valid when the volume is large, as we always assume, and when $h^{2,1} \gg 1$, which is precisely the region we are interested in.

3.1 Supersymmetric Minimum

Following the approach in [7], we stabilize the dilation $S = s + ia$ and complex structure moduli $U_j = u_j + i\nu_j$ at the SUSY point to find $W_0|_{\min}$ and then insert it into the superpotential W for the multi-Kähler moduli stabilization where SUSY will be broken due to the non-perturbative effects. To find the supersymmetric values for U_i and S , we have $D_S W_0 = \partial_S W_0 + \partial_S K W_0 = 0$ and $D_{U_i} W_0 = 0$, or

$$\text{Re}(D_S W_0) = \text{Re}(D_{U_i} W_0) = 0, \quad (3.2)$$

$$\text{Im}(D_S W_0) = \text{Im}(D_{U_i} W_0) = 0. \quad (3.3)$$

For $s > 1$, (3.2), (3.3) have solutions so the imaginary modes decouple in (3.2). So it is most convenient to work with the $a = \nu_i = 0$ solution for the imaginary modes and focus on the real parts of the moduli fields in the region $s > 1$ (for weak coupling) and $u_i > 0$ (to ensure that $K_{\text{cs+d}}$ stays real). Now W_0 becomes (defining $N_{\text{cs}} \equiv h^{2,1}$ for convenience)

$$W_0 = (c_1 - sc_2) + \sum_{i=1}^{N_{\text{cs}}} (b_i - sd_i)u_i \quad (3.4)$$

and $D_S W_0 = 0$ and $D_{U_i} W_0 = 0$ yield (assuming $s \neq 0$ and $u_i \neq 0$)

$$(c_1 + sc_2) + \sum_{i=1}^{N_{\text{cs}}} (b_i + sd_i)u_i = 0, \quad (3.5)$$

$$(c_1 - sc_2) - (b_i - sd_i)u_i + \sum_{j \neq i}^{N_{\text{cs}}} (b_j - sd_j)u_j = 0. \quad (3.6)$$

Now $N_{\text{cs}} = 0$ and $N_{\text{cs}} = 1$ are special cases and are easy to solve. So let $N_{\text{cs}} \geq 2$. We shall see that $N_{\text{cs}} = 2$ is also special. (3.6) immediately gives

$$v \equiv (b_1 - sd_1)u_1 = (b_2 - sd_2)u_2 = \cdots = (b_{N_{\text{cs}}} - sd_{N_{\text{cs}}})u_{N_{\text{cs}}}. \quad (3.7)$$

So u_i are solved in terms of s and one of them, say u_1 , or equivalently, v . Then (3.6) becomes

$$(c_1 - sc_2) + (N_{\text{cs}} - 2)v = 0, \quad (3.8)$$

and thus

$$W_0|_{\min} = -2 \frac{c_1 - sc_2}{N_{\text{cs}} - 2} = 2v, \quad (3.9)$$

where the second form is also applicable to the $N_{\text{cs}} \neq 0$ cases. We see that $s = c_1/c_2$ for $N_{\text{cs}} = 2$.

Now we have two equations (3.5) and (3.8) for two unknowns, v (or u_1) and s , and we have for $N_{\text{cs}} \neq 2$,

$$(N_{\text{cs}} - 2) \frac{c_1 + sc_2}{c_1 - sc_2} = \sum_{i=1}^{N_{\text{cs}}} \frac{b_i + sd_i}{b_i - sd_i} = \sum_{i=1}^{N_{\text{cs}}} \frac{1 + sr_i}{1 - sr_i}. \quad (3.10)$$

where $r_i = d_i/b_i$. In general, we cannot solve analytically for s . However, once s is determined by (3.10), we can express $W_0|_{\min}(N_{\text{cs}})$ in terms of s ,

$$w_0 \equiv W_0|_{\min}(N_{\text{cs}}) = -\frac{2(c_1 + sc_2)}{\sum_{i=1}^{N_{\text{cs}}} (1 + sr_i)/(1 - sr_i)} = -\frac{2(c_1 + sc_2)\prod_{i=1}^{N_{\text{cs}}} (b_i - sd_i)}{\sum_{i=1}^{N_{\text{cs}}} (b_i + sd_i)\prod_{j \neq i} (b_j - sd_j)}. \quad (3.11)$$

This is the formula quoted in the Introduction. Recall that we like s to be large and positive, say $s \approx \mathcal{O}(10)$. For the $N_{\text{cs}} = 0, 1, 2$ cases:

$$\begin{aligned} W_0|_{\min}(N_{\text{cs}} = 0) &= 2c_1, \quad s = -\frac{c_1}{c_2}, \\ W_0|_{\min}(N_{\text{cs}} = 1) &= -2\frac{(c_1 + sc_2)(b_1 - sd_1)}{b_1 + sd_1}, \quad s = \sqrt{\frac{c_1 b_1}{c_2 d_1}}, \\ W_0|_{\min}(N_{\text{cs}} = 2) &= -\frac{(c_1 + sc_2)(b_1 - sd_1)(b_2 - sd_2)}{b_1 b_2 - s^2 d_1 d_2}, \quad s = \frac{c_1}{c_2}. \end{aligned} \quad (3.12)$$

In appendix C, we further discuss the solution for s in special cases.

Treating c_j , b_j and d_j as random parameters, we allow them to take values such that each solution satisfies $s > 1$ and $u_i > 0$. We see that the each factor $(b_j - sd_j)$ in the numerator in (3.11) is allowed to pass through zero. We will check numerically that there is actually a peaking behavior as the number of complex structure moduli increases.

Before introducing the next-leading order terms (both non-perturbative and the $\hat{\xi}$ term) to generate a potential for the Kähler moduli, the model has a no-scale structure so $|D_{T_k} W|^2 = 3|W|^2$. Since $V = e^K \sum_i |D_i W|^2$ (with i running over complex structure moduli and dilaton) is semi-positive definite (with the supersymmetric minimum at $V = 0$), the Hessian (mass squared matrix) is semi-positively definite, owing to the no-scale structure. On the other hand, some of masses for the axionic modes turn out to be zero as discussed in [7]. Presumably, the non-perturbative corrections will generate cosine-like potentials, thus stabilizing the axionic fields.

The above values for s and u_i are solved at the supersymmetric point. Their values will be shifted after supersymmetry breaking [7]. The corrections are estimated of order

$$\frac{\delta(s, u_i)}{s, u_i} \sim \mathcal{O}\left(\frac{\hat{\xi}}{\mathcal{V}}\right). \quad (3.13)$$

As we reviewed in section 2.2, the expansion of $\mathcal{O}(\hat{\xi}/\mathcal{V})$ is compatible with the analysis for smaller Λ , and thus we can neglect the small correction to the complex structure sector in our analysis. It is worth commenting about the situation that total summed over corrections with large N_{cs} is not negligible. In this case, the extremal condition in the perturbation $\partial_{\phi_i} \partial_{\phi_j} V \cdot \delta\phi_j = -\partial_{\phi_i} \delta V$ suggests roughly

$$\delta(s, u_i) \propto \mathcal{O}\left(\frac{1}{N_{\text{cs}}}\right). \quad (3.14)$$

Therefore the correction may be suppressed by large N_{cs} instead.

3.2 Some properties of $w_0 = W_0|_{\min}$

We see that w_0 (3.11) together with the solution for s (3.10) have some interesting properties.

- Since c_1, c_2, b_j, d_j are random variables, so, for any fixed j , $(b_j - sd_j) \rightarrow 0$ is surely allowed. (3.10) for s indicates that when $(b_j - sd_j) \rightarrow 0$ for any j , the RHS blows up (in the absence of delicate cancellations) so LHS requires $s \rightarrow c_1/c_2$. Now, in the vicinity of $b_j - sd_j = 0$, s becomes independent of the other values of (b_i, d_i) for $i \neq j$.
- The factors $(b_i - sd_i)$ appear in the numerator of w_0 (3.11). Knowing that $s \rightarrow c_1/c_2$ is insensitive to (b_i, d_i) for $i \neq j$ in the vicinity of $(b_j - sd_j) = 0$, we can work out the probability distribution $P(z)$ for $z = b_i - sd_i$ for $i \neq j$,

$$P(z) = \int_0^1 \int_0^1 db_i dd_i \delta((b_i - sd_i) - z). \quad (3.15)$$

A careful treatment of the limits of integration yields,

$$P(z) = \begin{cases} (1-z)/s, & 0 \leq z \leq 1, \\ 1/s, & 1-s \leq z \leq 0, \\ 1+z/s, & -s \leq z \leq 1-s. \end{cases} \quad (3.16)$$

and $P(z) = 0$ outside. This distribution has the shape of a trapezoid and $P(0) = 1/s$. (It follows that $\langle z \rangle = (1-s)/2$.) This implies that when $(b_j - sd_j) \rightarrow 0$, the probability that $(b_i - sd_i) \rightarrow 0$ for any $i \neq j$ is not suppressed. Furthermore, the individual $(b_i - sd_i) \rightarrow 0$ approach are more or less independent, so the $n = N_{\text{cs}}$ th order zero is within the parameter ranges we are interested in and we may intuitively expect a peaking behavior

$$P(w_0) \propto (\ln |w_0|)^{N_{\text{cs}}-1} \quad \text{as} \quad w_0 \rightarrow 0. \quad (3.17)$$

- Let $r_i = d_i/b_i$. At the symmetry point where all r_i are equal, $r_1 = r_2 = \dots = r_{N_{\text{cs}}} = r$, we see that $W_0|_{\min}(N_{\text{cs}})$ (3.11) collapses to

$$W_0|_{\min}(N_{\text{cs}}) = -\frac{2(c_1 + sc_2)(1 - sr)}{N_{\text{cs}}(1 + sr)}. \quad (3.18)$$

As r sweeps pass $1/s$, we obtain only a single zero in w_0 . For this symmetry point, we expect $P(w_0)$ to be smooth at $w_0 = 0$. That is, the peaking behavior (3.17) will disappear if we restrict ourselves to the symmetry point. So if the peaking behavior in $P(w_0)$ is to survive, it must come from the vicinity of the symmetry point, which has a bigger region of parameter space than that of the symmetry point. Away from this symmetry point, some zeros in the numerator of w_0 (3.11) may be canceled by coincident zeros in the denominator of w_0 (3.11), depending on the choice of the random parameters. This may lead to some transient behavior in $P(w_0)$. Solution for s at the symmetry point is discussed in appendix C.

- Constraint among the parameters comes into play as we limit the range of s so the weak coupling approximation is valid. This will also introduce some transient behavior in $P(w_0)$. This transient behavior should fade away as we go to large N_{cs} .
- Note that both the expression for s (3.10) and the expression for w_0 (3.11) are invariant under the simultaneous rescaling $b_i \rightarrow \lambda_i b_i$ and $d_i \rightarrow \lambda_i d_i$, so $P(w_0)$ should be unchanged when we change the range of both b_i and d_i by a factor of λ_i . Recall the example (2.3) where the expectation value strongly depends on the range of the random variables. This would be very unsatisfactory here since we do not know the reasonable ranges for (b_i, d_i) . Fortunately, because of this λ_i scaling property, we see that both $P(w_0)$ and $\langle w_0^p \rangle$ are insensitive to the rescaling of the (b_i, d_i) ranges. We shall find some reasonable choices of ranges for b_i when we come to the potential V and $P(\Lambda)$. Here, we restrict ourselves to $w_0 < 0$ so we simply need to look at only $\langle w_0 \rangle$ (instead of $\langle w_0^2 \rangle$). Suppose we take the range of c_i to be $[-r_{\text{cutoff}}, +r_{\text{cutoff}}]$, then $\langle w_0 \rangle / r_{\text{cutoff}}$ is independent of r_{cutoff} and the ranges of b_i, d_i . For example, for $N_{cs} = 5$, we have $\langle w_0 \rangle / r_{\text{cutoff}} \simeq -2$.

Overall, we expect that $P(w_0)$ peaks more sharply at $w_0 = 0$ as N_{cs} increases; however, we do not know analytically the precise peaking behavior of $P(w_0)$.

So we expect that the expectation value $\langle w_0 \rangle$ decreases as N_{cs} increases. Because of the nontrivial forms of s (3.10) and w_0 (3.11), it is crucial to find their behaviors numerically.

3.3 Numerical comparison of w_0

In the above analysis, we see the product type of structure in $W_0|_{\min}$ (3.11). However, since the parameters in the denominator are not independent of those in the numerator, it is important to perform numerical analysis and check whether the distribution does become more sharply peaked as we increase the number of complex structure moduli.

Now we impose a randomness in the model (3.4). Given random values for c_1, c_2, b_i, d_i obeying uniform distribution, we solve supersymmetric conditions $D_S W_0 = 0, D_{U_i} W_0 = 0$ for real part of moduli fields, s, u_i . Here we restrict ourselves in $-1 \leq c_1, c_2, b_i, d_i \leq 1$ for just a choice. We are also interested in the region where string coupling $g_s = e^\phi = s^{-1}$ can be treated perturbatively, therefore we further impose $s > 1$ together with $u_i > 0$ (which is required for a real-valued Kähler potential in our definition).

Recall that the $w_0 A_1 < 0$ condition is required for the Kähler moduli stabilization with positive Λ as we see in section 2.2. Because of the reflection symmetry, we may focus on the $w_0 < 0$ region without losing generality here. It is worth commenting that all of the numerical solutions obtained just by solving the supersymmetric condition actually satisfy the positivity of the Hessian. Thus we can insert the solution in the model for the Kähler moduli stabilization.

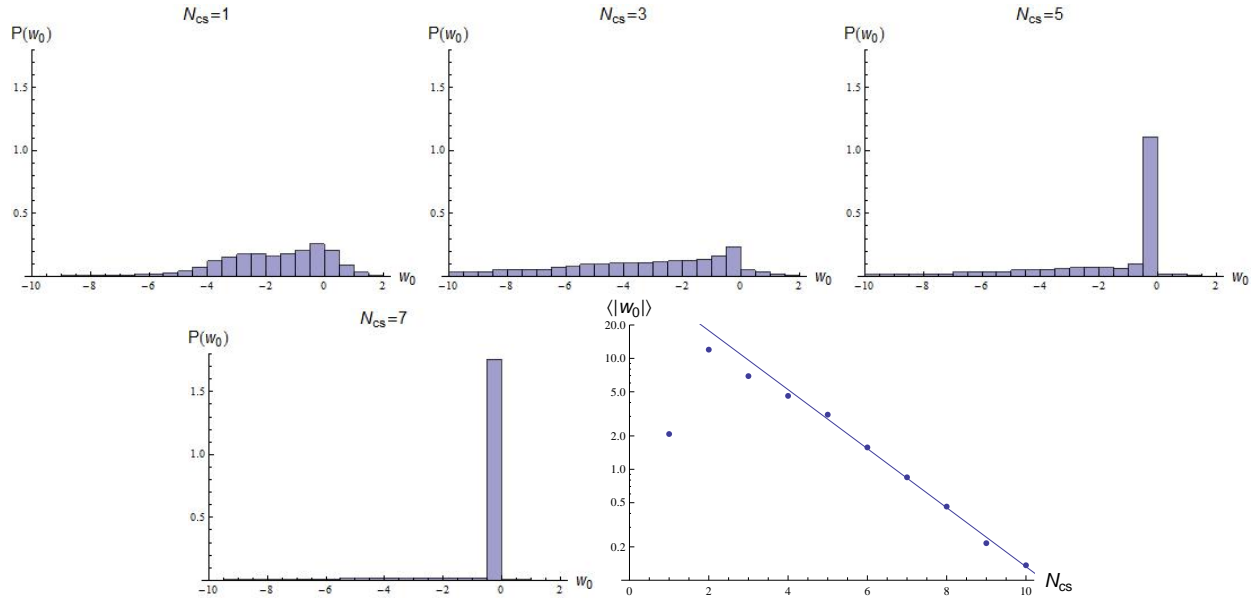


Figure 8: The probability distribution $P(w_0)$ for $-10 \leq w_0 \leq 2$ with fixed $b_i = -1$ at $N_{cs} = 1, 3, 5, 7$ respectively. In the last figure, we show the behavior of the expectation value $\langle |w_0| \rangle$ for $N_{cs} \leq 10$.

Inserting the solutions for s (3.10) and u_i (3.7) into $w_0 = W_0|_{\min}$ (3.11), we obtain the distribution $P(w_0)$ and its behavior. In Figure 1, we show the resultant probability distribution $P(w_0)$ for various $h^{2,1} = N_{cs}$, where the dilaton dependence has been taken into account. Because of the non-trivial dependence in the denominator of (3.11), the peak at $w_0 = 0$ is smoothed out around $N_{cs} = 3, 4$, but emerges at $N_{cs} \geq 5$. For $N_{cs} \geq 5$, the peak at $w_0 = 0$ becomes sharper as we increase N_{cs} . Although W_0 (3.4) takes the form of a sum of terms and therefore one might expect a sum distribution (which is smooth at $W_0 = 0$, as shown in Figure 2), instead of a product distribution (which typically peaks at 0), the data clearly shows a sharper peak in $P(w_0)$ (Figure 1) as we increase the number of complex structure moduli. This is nothing but the outcome of the correlation of the terms through the stabilization of complex structure moduli and dilaton.

Although the distribution feature for the parameters c_1, c_2, b_i, d_i are reasonably well-motivated from the flux compactification because these parameters are from the 3-form fluxes H_3, F_3 , we like to consider other possibilities. Since $u_i = w_0/2b_i(1 - sr_i)$, allowing $b_i = 0$ implies that we are looking at vacua where some $u_i \rightarrow \infty$, which may not be valid within our approximation. So, as an alternative, let us restrict the values of b_i to a range that excludes zero, say $0 > -f_{\min} \geq b_i \geq -f_{\max}$. It turns out that the qualitative physics does not change if we simply restrict b_i to a fixed value, say $b_i = -f < 0$, where we may consider $-f$ to be the average value of b_i with a range. Note that u_i stays finite as $(1 - sr_i) \rightarrow 0$, since $w_0 \rightarrow 0$ in this limit as well.

Again, we can solve for $s > 1$ and $u_i > 0$ and determine w_0 . In Figure 8, we show the distributions of $P(w_0)$ with fixed $b_i = -1$ while allowing the other parameters uniformly dis-

tributed with the range $-1 \leq c_1, c_2, d_i \leq 1$. We again impose the weak string coupling constraint $s > 1$ as well as $u_i > 0$. As apparent from the comparison between Figure 1 and Figure 8, the distribution of w_0 in this case is more peaked toward $w_0 = 0$. Note that the distribution for $w_0 > 0$ is quite different from that for $w_0 \leq 0$ in this setup. This is because the sign fixing of b_i violates the reflection symmetry of w_0 (realized by flipping signs of all the parameters c_i, b_i, d_i simultaneously in the model).

We also estimate the expectation value $\langle |w_0| \rangle$ as a function of N_{cs} , especially for $N_{\text{cs}} = 4 - 10$. In an attempt to extract the large N_{cs} behavior, we neglect the data points for $N_{\text{cs}} < 4$, because of the transient behavior at lower N_{cs} . The data points (for $N_{\text{cs}} \geq 4$) in Figure 8 are well fitted by $\langle |w_0| \rangle = 60.6 e^{-0.613 N_{\text{cs}}}$. However, numerical data indicates that the drop of $\langle |w_0| \rangle$ as a function of N_{cs} slows down as we go to $N_{\text{cs}} > 10$ (see LHS of Figure 4).

The peaking behavior of $P(|w_0|)$ may be quantified via a comparison of the values at a fixed percentage of $|w_0|$ accumulating from the zero point. Let us introduce $|w_0|^{Y\%}$ defined by $\int_0^{|w_0|^{Y\%}} P(|w_0|) d|w_0| = Y\%$. That is, there is a $Y\%$ chance that $|w_0|$ will be smaller than $|w_0|^{Y\%}$. In LHS of Figure 4, we show $\langle |w_0| \rangle$, $|w_0|^{80\%}$ and $|w_0|^{10\%}$ as a function of N_{cs} in the range $1 \leq N_{\text{cs}} \leq 30$. We see that, for $N_{\text{cs}} > 3$, they all decrease as the number of complex structure moduli increases.

3.4 Inserting the w_0 solution into the single Kähler modulus model

Now we consider the moduli stabilization in the presence of single Kähler modulus, given the data of w_0, s, u_i obtained by solving supersymmetric conditions for complex structure and dilaton moduli. The potential we have in mind here is given by

$$\begin{aligned} K &= -2 \ln \left(\mathcal{V} + \frac{\hat{\xi}}{2} \right) - \ln(2s) - \sum_i^{h^{2,1}} \ln(2u_i), \\ \mathcal{V} &= \gamma_1 (T_1 + \bar{T}_1)^{3/2}, \quad \hat{\xi} = -\frac{2\zeta(3)}{3(2\pi)^3} s^{3/2} 2(h^{1,1} - h^{2,1}), \\ W &= w_0 + A_1 e^{-a_1 T_1}. \end{aligned} \tag{3.19}$$

We consider the stabilization of single Kähler moduli with the potential above, under the assumption of complex structure moduli stabilization at higher energy, which is not affected by the next leading order corrections for Kähler modulus stabilization. Again, we choose the solution where $\text{Im} T_1 = 0$ and focus on $t_1 = \text{Re} T_1$. The potential above has additional contribution in the overall factor in addition to (2.5), which is estimated by

$$\begin{aligned} V &\sim \frac{-w_0 a_1^3 A_1}{2\gamma_1^2 2^{N_{\text{cs}}+1} s \prod u_i} \left(\frac{2C}{9x_1^{9/2}} - \frac{e^{-x_1}}{x_1^2} \right), \\ C &= \frac{-27w_0 \hat{\xi} a_1^{3/2}}{64\sqrt{2}\gamma_1 A_1}, \quad x_1 = a_1 t_1, \end{aligned} \tag{3.20}$$

where we approximate the potential up to linear order of $\hat{\xi}/\mathcal{V}$, $A_1 e^{-x_1}/W_0$, and $N_{\text{cs}} = h^{2,1}$ just for convenience. Here, we set $a_1 = \gamma_1 = 1$ for simplicity.

In this section, we present the data obtained for the following 4 cases :

1. $-1 \leq c_1, c_2 \leq 1, \quad -f_1 \leq b_i, d_i \leq f_1,$
2. $-1 \leq c_1, c_2, r_i = b_i/d_i \leq 1 \quad -f_2 \leq b_i \leq f_2,$
3. $-1 \leq c_1, c_2 \leq 1, \quad b_i = \pm f_3, \quad -f_3 \leq d_i \leq f_3,$
4. $-1 \leq c_1, c_2 \leq 1, \quad b_i = -f_4, \quad -f_4 \leq d_i \leq f_4,$

with uniform distributions for the ranges of the random parameters as shown. Note that we impose uniform distribution for r_i instead of d_i in Case 2. The positively defined parameter f_j will be fixed later. For each case, we insert the given distributions into (3.1) and solve for the supersymmetric conditions (3.2) for s, u_i, w_0 , and collect sets of data for $s > 1, u_i > 0$. The invariance under rescaling b_i, d_i simultaneously in (3.11), the peaking behavior of $w_0 \leq 0$ as well as the distribution itself is independent of f_j .

As we have discussed in the previous subsection, we observe the peaking behavior in w_0 as N_{cs} increases. However, we also see that $P(u_i)$ are also peaked toward $u_i = 0$, and therefore the coefficient of the potential $V(3.20)$ goes essentially infinity, meaning that the resultant Λ itself may diverge. Since we use the effective potential for the 4D gravity analysis, the maximal value of the potential should be within the Planck scale for it to be valid within the approximation used. Since $V(x_1 = 0)$ blows up, it makes more sense to use the barrier height as a measure of the scale of the potential. The easiest way to implement this constraint is for the barrier height (2.11) to be no higher than the Planck scale, or

$$V_H \equiv \frac{1}{9} \left(\frac{2}{5} \right)^{9/2} (0.24) \frac{-w_0 A_1}{2^{N_{\text{cs}}+1} s \prod u_i} \leq 1. \quad (3.21)$$

That is, we keep only those V_H that are less than unity. Here we give A_1 an uniform distribution in the range $-1 \leq A_1 \leq 1$. To enhance the data sample without changing the underlying physics, we may simply restrict ourselves to small values of f_i , where $V_H \propto f_j^{N_{\text{cs}}}$. There may be a number of different ways to choose the cutoff point. Here we employ a specific way to achieve this: we count the number of data starting from $V_H = 0$, and we choose f_i so that 90% of $V_H \leq 1$, then we set this as the cutoff point and keep only this $V_H \leq 1$. This implies that we restrict ourselves to the cases where $\Lambda \lesssim 1$. Note that we do not lose generality by the restriction $w_0 \leq 0$ for Case 1-3, since we have the reflection symmetry of w_0 by changing the signs of all parameters c_i, b_i, d_i , which remains solutions for s, u_i unchanged. Changing the 90% cutoff to a higher or slightly lower value does not change the qualitative picture.

Let us estimate f_j in each case. To keep 90% of $V_H \leq 1$, we need to choose a smaller f_j as N_{cs} increases. In LHS of Figure 9, we show the plot for the value of f_j required to normalize the

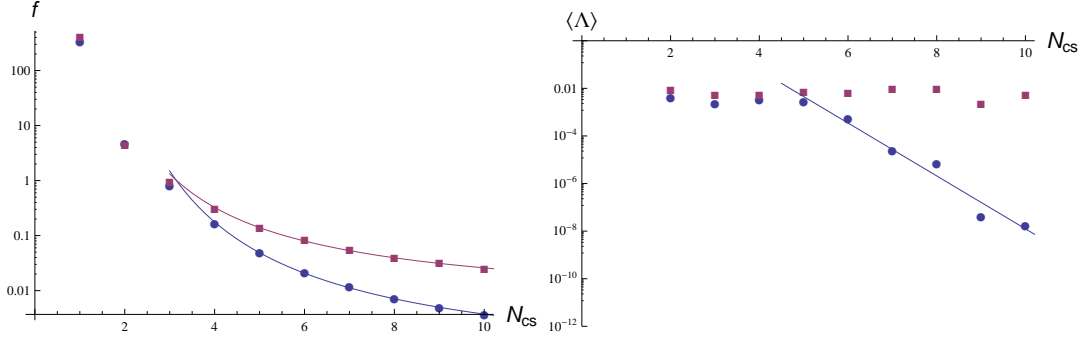


Figure 9: The estimated values of f_k and $\langle \Lambda \rangle$ in Case 1 (purple, rectangular) and Case 4 (blue, circle). The fitting curves here are $f_1 \sim e^{-5.33+16.9/N_{cs}}$ (red on LHS), $f_4 \sim e^{-8.16+25.7/N_{cs}}$ (blue on LHS) and $\langle \Lambda \rangle_4 \sim e^{-2.56N_{cs}+7.40}$ (blue on RHS). However, the drop of $\langle \Lambda \rangle$ as a function of N_{cs} slows down appreciably for larger values of N_{cs} .

cutoff point of V_H in Case 1, 4 just for illustration. For $N_{cs} \geq 4$, f_j may be estimated to be :

$$f_1 \sim e^{-5.33+16.9/N_{cs}}, \quad f_2 \sim e^{-4.62+20.5/N_{cs}}, \quad f_3 \sim e^{-5.78+19.6/N_{cs}}, \quad f_4 \sim e^{-8.16+25.7/N_{cs}}. \quad (3.22)$$

We see that $f_i \ll 1$ at larger N_{cs} .

Now we are ready to plug the data into (3.20). Since we consider just the single Kähler modulus stabilization with the sets of data inputs, the stabilization mechanism follows that reviewed in section 2.2, where the combined parameters obey $3.65 \lesssim C < 3.89$ for metastable dS vacua. First we give A_1 an uniform distribution with range $-1 \leq A_1 \leq 1$. Next we choose the data for one of the four cases mentioned above for each fixed N_{cs} . The probability distribution $P(\Lambda)$ of Λ in Case 1 is illustrated in Figure 3. We see that there is the clear peaking behavior toward $\Lambda = 0$, which is getting sharper as N_{cs} increases. However, we do not see any clear trend for $\langle \Lambda \rangle$ in RHS of Figure 9. This is probably because there is a non-trivial long tail in large Λ in $P(\Lambda)$ which contribute significantly to $\langle \Lambda \rangle$. In Case 2 and 3, we see a clear peaking of $P(\Lambda)$ at $\Lambda = 0$, similar to that in Case 1; but again $\langle \Lambda \rangle$ behaves quite similarly to that in Case 1, without a clear trend one way or another.

Next, let us consider Case 4, with $b_i = -f_4$ and $w_0 \leq 0$. The result is shown in Figure 9. The peaking behavior of $P(\Lambda)$ at $\Lambda = 0$ is again evident, while $\langle \Lambda \rangle$ has a rather different behavior than the other 3 cases. The $\langle \Lambda \rangle$ in Case 4 is shown in Figure 4. We find that it is roughly given by

$$\langle \Lambda \rangle_4 \sim e^{-2.56N_{cs}+7.40} \quad (3.23)$$

for $N_{cs} \leq 10$. However, the drop in $\langle \Lambda \rangle$ slows appreciably for $N_{cs} > 10$ as showed in RHS of Figure 4. Still, this example illustrates the sensitivity of $\langle \Lambda \rangle$ to the input ranges and distributions of the random parameters.

Similarly to w_0 , we can quantify the peaking behavior of $P(\Lambda)$ by estimating the value at a fixed percentage of data counting from $\Lambda = 0$. Let us introduce $\Lambda^{Y\%}$, defined by $\int_0^{\Lambda^{Y\%}} P(\Lambda) d\Lambda =$

$Y\%$. That is, there is a $Y\%$ chance that Λ will fall in the range $\Lambda^{Y\%} \geq \Lambda \geq 0$. In Figure 4, we show $\langle \Lambda \rangle$, $\Lambda^{80\%}$ and $\Lambda^{10\%}$ as a function of the number of complex structure moduli. For example, at $N_{\text{cs}}(\equiv h^{2,1}) = 20$, while $\langle \Lambda \rangle \simeq 1.2 \times 10^{-8}$, we have $\Lambda^{80\%} \simeq 2.0 \times 10^{-19}$ and $\Lambda^{10\%} \simeq 4.8 \times 10^{-28}$. Although the drop of $\langle \Lambda \rangle$ is quite mild after $N_{\text{cs}} > 10$, we see that $\Lambda^{80\%}$ and $\Lambda^{10\%}$ continue to drop appreciably. This means that most Λ have small values, while there exist a long tail $\Lambda \lesssim 1$ in the distribution $P(\Lambda)$.

By choosing smaller $|b_i|$ allows us to accumulate more data. What happens if we impose a different cutoff on V_H . As an example, let us choose b_i so that, instead of 90%, only 20% of the potentials have $V_H \leq 1$. That is, the potentials are less squeezed to small values in the 20% cutoff scenario. In this case, we find that, for $N_{\text{cs}} = 20$, $\Lambda^{80\%} \simeq 8.6 \times 10^{-6}$ and $\Lambda^{10\%} \simeq 1.2 \times 10^{-9}$, which are substantially bigger than those for the 90% cutoff case. Clearly we have to understand this squeezing issue better.

So far we have considered the physical quantities Λ and the related potential barrier V_H in this subsection. However, one may also consider, instead of V_H , the quantity $e^{K_{\text{cs+d}}} |W_0|^2$, which is invariant under the Kähler transformation. The Kähler invariant quantity at a minimum is given by $e^{K_{\text{cs+d}}} |W_0|^2 = w_0^2 / (2^{N_{\text{cs}}+1} s \prod u_i)$. Since this quantity may diverge due to the u_i in the denominator (as in the case of V_H), we need to introduce the cutoff to make this quantity within Planck scale (this quantity is a term in the potential). If we follow the same procedure as that for V_H , the distribution of the Kähler invariant quantity at each N_{cs} suggests sharply peaked distribution, which is qualitatively similar to what we have seen already for $P(\Lambda)$.

3.5 Some remarks

A few remarks may be in order here:

- Note that the “product” form emerges in the superpotential value w_0 (3.11), despite the fact that the parameters b_i and d_i appear in the “sum” form in the original superpotential (3.1). As pointed out in [3], any linear combination of a set of random variables, as naively the case in (3.1), will not yield a peaking behavior. That is, W_0 will be smooth at zero if the u_i , the real part of U_i in W_0 are treated as independent arbitrary constants. When we go to the supersymmetric point for the minimum, u_i become functions of b_i and d_i , which leads to the product form in (3.11). It is the (complex structure and dilation) moduli stabilization dynamics that converts the “sum” form (3.1) to the “product” form (3.11), which is the key to the peaking property of $P(w_0)$ and $P(\Lambda)$, the latter of which is necessary for the stringy mechanism for a naturally small Λ to work.
- The actual values of u_i and s will surely be shifted away from the supersymmetric point after supersymmetry breaking. The correction of back reaction to the set of solutions is suppressed due to the suppression of large volume and larger W_0 compared to the non-

perturbative terms if we work in this parameter region [7]. Even if we include the corrections in W_0 , the modification would be negligible and therefore the feature of peaked behaviors should remain intact.

- It is possible (even likely) that the coefficient A_k in (1.1) emerges as a consequence of the stabilization of higher scale moduli. In this case, we expect the probability distribution $P(A_k)$ to be peaked at $A_k = 0$. This will enhance the peakiness of $P(\Lambda)$, so fewer complex structure moduli may be needed for a small enough Λ .
- Both the model and its solution we study here are simple enough for a clear analysis. This opens some questions on the simplifications we are taking. There are additional interaction terms in both W and K coming from higher order corrections. Based on the limited experience we have developed so far, one may hope that those (higher α' or stringy loop [13, 26, 27]) corrections will lead to tighter interactions among the moduli and so will actually strengthen the peaking behaviors. However, this does not necessarily imply an exponentially small Λ .

4 Multi-Kähler moduli cases

A model for multiple Kähler moduli stabilization at positive Λ is even suggested especially with non-perturbative effects in superpotential and α' correction in Kähler, considered in [5–8] or known as *Kähler uplifting model*. The model basically assumes the stabilization of the complex structure moduli and dilaton-axion moduli at high scale, while the Kähler moduli stabilization is achieved at low energy scale with the non-perturbative effect and the α' -correction. Together with the non-trivial constant W_0 in the superpotential, given after complex and dilaton moduli stabilization, we can have a small positive minimum as a result of Kähler moduli stabilization.

We consider the supergravity effective potential which is obtained after the Calabi-Yau compactification in type IIB:

$$\begin{aligned}
K &= -2 \ln \left(\mathcal{V} + \frac{\hat{\xi}}{2} \right), \quad \mathcal{V} = \gamma_1 (T_1 + \bar{T}_1)^{3/2} - \sum_{i=2}^{N_K} \gamma_i (T_i + \bar{T}_i)^{3/2}, \\
W &= W_0 + \sum_{i=1}^{N_K} A_i e^{-a_i T_i},
\end{aligned} \tag{4.1}$$

where we have again introduced the non-perturbative terms proportional to A_i for all of $N_K = h^{1,1}$ Kähler moduli, and the α' correction defined $\hat{\xi} = -\zeta(3)\chi(M)/(4\sqrt{2}(2\pi)^3)$. We basically require $\hat{\xi} > 0$ for the stability analyses later, meaning that the number of complex structure moduli is greater than the number of Kähler moduli: $\chi(M) = 2(h^{1,1} - h^{2,1}) < 0$. W_0 comes from the flux contributions, and generically does not depend on Kähler moduli (no-scale structure).

We assume that the non-perturbative effect and the α' correction are small enough compared to the other quantities as well as in section 2.2, so that we analyze the potential up to linear orders of

$$\frac{\hat{\xi}}{\mathcal{V}} \ll 1, \quad \left| \frac{A_i e^{-a_i T_i}}{W_0} \right| \ll 1. \quad (4.2)$$

These assumptions are quite natural since the α' correction can be treated to be small in perturbation theory. As we see in the previous section, this perturbative analysis agrees with the analysis for small Λ . There are essentially two important outcomes of these assumptions: (1) suppression of the off-diagonal components between the Kähler components and the complex structure/dilaton components in the mass matrix, and (2) simplification of the potential for the Kähler moduli since we can neglect the next-to-next leading order in the potential with respect to the approximation (4.2).

We focus on the real part of Kähler moduli $\text{Re } T_i = t_i$ because the imaginary part always has a potential of cosine type and therefore $\text{Im } T_i = 0$ always satisfy the extremal conditions. The $\text{Im } T_i = 0$ solutions also decouple the real sector from the imaginary sector completely in the mass matrix [7]. Thus we can safely neglect the imaginary components.

The potential is expanded with respect to (4.2), so

$$V \sim \frac{3W_0^2 \hat{\xi}}{64\sqrt{2}\mathcal{V}^3} + \sum_{i=1} \frac{a_i t_i A_i e^{-a_i t_i} W_0}{2\mathcal{V}^2}. \quad (4.3)$$

Defining the following parameters:

$$x_i = a_i t_i, \quad \delta_i = \frac{\gamma_i a_i^{-3/2}}{\gamma_1 a_1^{-3/2}}, \quad C = \frac{-27W_0 \hat{\xi} a_1^{3/2}}{64\sqrt{2}\gamma_1 A_1}, \quad B_i = \frac{A_i}{A_1}, \quad (4.4)$$

the potential takes the approximate form:

$$V \sim -\frac{A_1 W_0 a_1^3}{2\gamma_1^2} \left(\frac{2C}{9(x_1^{3/2} - \sum_{j=2} \delta_j x_j^{3/2})^3} - \frac{x_1 e^{-x_1}}{(x_1^{3/2} - \sum_{j=2} \delta_j x_j^{3/2})^2} - \sum_{i=2} \frac{B_i x_i e^{-x_i}}{(x_1^{3/2} - \sum_{j=2} \delta_j x_j^{3/2})^2} \right). \quad (4.5)$$

Here, we have a symmetry of exchanging moduli fields x_i together with the assigned parameters B_i , coming from the symmetry for T_i ($i \neq 1$) which the full potential (4.1) contains.

Our purpose here is twofold : to study (1) the effect of increasing the number $h^{1,1}$ of Kähler moduli and (2) the effect of different distributions for W_0 and A_i , on both $P(\Lambda)$ and $\langle \Lambda \rangle$. For the first case, we shall simply treat W_0, A_i as random parameters with uniform distributions.

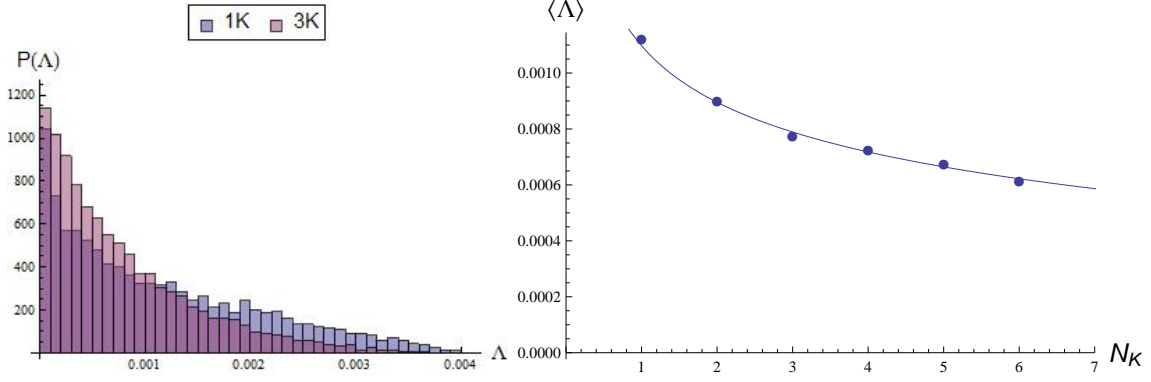


Figure 10: The probability distribution $P(\Lambda)$ of Λ assuming uniformly distributed W_0, A_i . $\langle \Lambda \rangle$ as a function of the number N_K of Kähler moduli; the curve is given by $\langle \Lambda \rangle \sim 0.00110 N_K^{-0.226} e^{-0.0268 N_K}$.

4.1 Uniformly distributed W_0, A_i

Now we find the meta-stable minimum of V (4.5) to obtain Λ and then estimate its probability distribution $P(\Lambda)$ and $\langle \Lambda \rangle$. Here again we set $a_i = \gamma_i = \hat{\xi} = 1$ to see just the effect of randomness of W_0, A_i on $P(\Lambda)$ and $\langle \Lambda \rangle$. We shall start with uniform distributions for the parameters W_0, A_i . Here we compare several different distributions with different setups to see how $P(\Lambda)$ and $\langle \Lambda \rangle$ behave.

First we assume uniformly distributed random parameters W_0, A_i with range: $-15 \leq W_0 \leq 0$, $0 \leq A_i \leq 1$ for convenience. The choice of sign here is for increasing chance of dS solutions. Even if we use the different choices, the resultant behavior is unchanged. The calculation cost for solving for t_i and checking the stability can be hugely reduced if we limit ourselves in the parameter region which is valid for meta-stable vacua at $\Lambda \geq 0$. We follow the analysis of the parameter region up to three-moduli in appendix D, and further apply the similar limitation for the models with more Kähler moduli. The limitation of our interest is the one we obtain in the case with three Kähler moduli, but we can expect the similar validity region for $B_i - B_j$ plane ($i \neq j$) as that of $B_2 - B_3$ plane, owing to the symmetry. This limitation hugely reduces our calculation costs so we can numerically get the statistical distributions of the potential (4.1) even at larger numbers of Kähler moduli.

In Figure 10, we show plots of the statistical analyses. If we assume uniformly distributed W_0, A_i , then the probability distribution $P(\Lambda)$ of Λ become more sharply peaked as the number N_K of Kähler moduli increases. The plot in RHS suggests that the expectation value $\langle \Lambda \rangle$ of Λ is suppressed as a function of N_K :

$$\langle \Lambda \rangle \sim 0.00110 N_K^{-0.226} e^{-0.0268 N_K}, \quad (4.6)$$

where we neglected the point at $N_K = 1$ in estimation, since the single modulus model does not have off-diagonal components in the Hessian, and therefore we expect that the value at $N_K = 1$

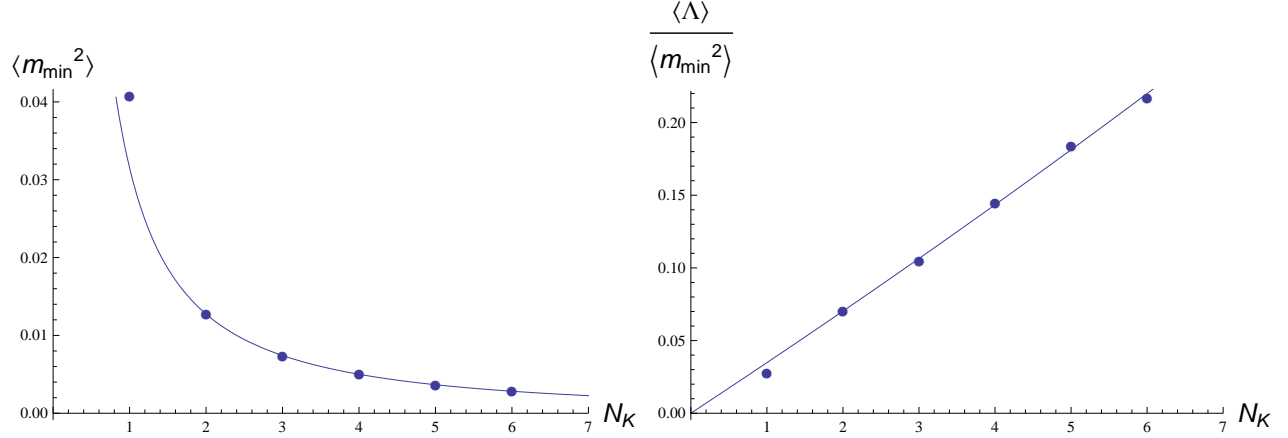


Figure 11: The expectation value of the lowest eigenvalue of the physical mass (squared) matrix and the ratio of the expectation values. The estimated curve on the LHS goes as $\langle m_{\min}^2 \rangle \sim 0.0317 N_K^{-1.21} e^{-0.0422 N_K}$. RHS gives the ratio $\langle \Lambda \rangle / \langle m_{\min}^2 \rangle$ as a function of N_K .

is not necessary to obey the estimated curve from the data among $N_K = 2 - 6$.

Although we see the suppression of $\langle \Lambda \rangle$ as increasing N_K , we may worry that the similar suppression happens even for mass terms, because the mass matrix is also given as a complicated function of the parameters and moduli. We now estimate the physical mass matrix, which is the mass matrix for canonically defined fields. The physical mass matrix is related to the second derivative of potential $\partial_{t_i} \partial_{t_j} V$ through the diagonalization matrix of Kähler metric. The diagonalization matrix D_{ij} of the Kähler metric is defined to satisfy

$$D_{ki} K_{ij} D_{jl}^T = \lambda_k \delta_{kl} \quad (4.7)$$

where λ_i are the eigenvalues of Kähler metric and same indices in LHS are summed over. Then the canonical coordinate Y_i is defined to be

$$dY_i = \sqrt{2\lambda_i} (D^T)_{ik}^{-1} dt_k. \quad (4.8)$$

Now we know the conversion matrix to physical mass matrix from the second derivative matrix:

$$m_{ij}^2 = \frac{dt_k}{dY_i} \frac{dt_l}{dY_j} \partial_{t_k} \partial_{t_l} V|_{\min}. \quad (4.9)$$

Performing the conversion at each stable point, we can calculate the physical mass matrix accordingly.

In the distribution of lowest eigenvalue of mass matrix, we see the more sharply peaked behavior as increase of N_K as well as the distribution of Λ . But as in Figure 11, the suppression effect is actually stronger than that for $\langle \Lambda \rangle$. The expectation value of the lowest eigenvalue m_{\min} is estimated as a function of N_K , again neglecting the point at $N_K = 1$, by

$$\langle m_{\min}^2 \rangle \sim 0.0317 N_K^{-1.21} e^{-0.0422 N_K}. \quad (4.10)$$

Now we see that the suppression of $\langle m_{\min}^2 \rangle$ is faster than the suppression of $\langle \Lambda \rangle$ because of the difference in the exponent. In addition to the similar suppression we have in Λ , the non-trivial off-diagonal components cause the eigenvalue repulsion in the mass matrix when the rank of the matrix gets higher. As a result of this, the minimal eigenvalue of mass matrix is further pushed down in general. This tendency can be read clearly from the RHS plot in Figure 11.

Once the lowest eigenvalue of mass matrix reaches smaller values, we may worry about the cosmological moduli problem [22–24], implying $m_{\min} \gtrsim \mathcal{O}(10) \text{ TeV} \sim 10^{-15} M_P$ ¹. In the current situation with uniformly distributed W_0, A_i , the lowest eigenvalue of mass matrix can be smaller than the Λ . Therefore we encounter the cosmological moduli bound $\langle m_{\min}^2 \rangle \sim 10^{-30}$ where $N_K \sim 1.35 \times 10^3$, earlier than the value for the current cosmological constant $\langle \Lambda \rangle \sim 10^{-122}$ where $N_K \sim 1.01 \times 10^4$.

4.2 Sharply peaked $P(W_0)$ and uniform distribution $P(A_i)$

Motivated by the analysis in previous subsection, it is quite possible that the parameters W_0, A_i themselves are given as products or non-trivial functions of random parameters as a result of the stabilization of the complex structure and dilaton moduli. As a toy model, let us consider a peaked distribution $P(W_0)$ for W_0 while A_i remain to have a uniform distribution as before. Motivated by the product distribution case (2.2), we simply assume

$$P(W_0) = \frac{1}{15(n-1)!} \left(\ln \frac{15}{|W_0|} \right)^{n-1}, \quad -15 \leq W_0 \leq 0, \quad (4.11)$$

where again the choice of sign does not affect the result. The number “15” is just a choice to increase the chance of getting dS solutions in the numerical simulation. As we see in (2.4), the expectation value of W_0 is exponentially suppressed in the presence of multiple random parameters.

Here we also assume that the values of s, u_i are given as roughly of order one, and therefore negligible. Even though we observe that the s, u_i behave differently in the simplest model for complex structure moduli stabilization in section 3.4, it is possible that the situation will be totally different in a different class of models for complex structure moduli stabilization. But since we do not have enough information of the other models, here we simply ignore the direct effect of s, u_i so that we can simply extract the effect of the combination between peaked distribution of W_0 and Kähler moduli dynamics.

In this setup, we solve the model numerically satisfying the stability constraint at positive Λ , up to $n = 5$ at each $N_K = 1, 2, 3$. The resultant plots are showed in Figure 12. The estimated

¹The stringent bound for the reheating temperature $T_r \gtrsim 0.7 \text{ MeV}$ comes from successful neutrino thermalization and BBN [28, 29].

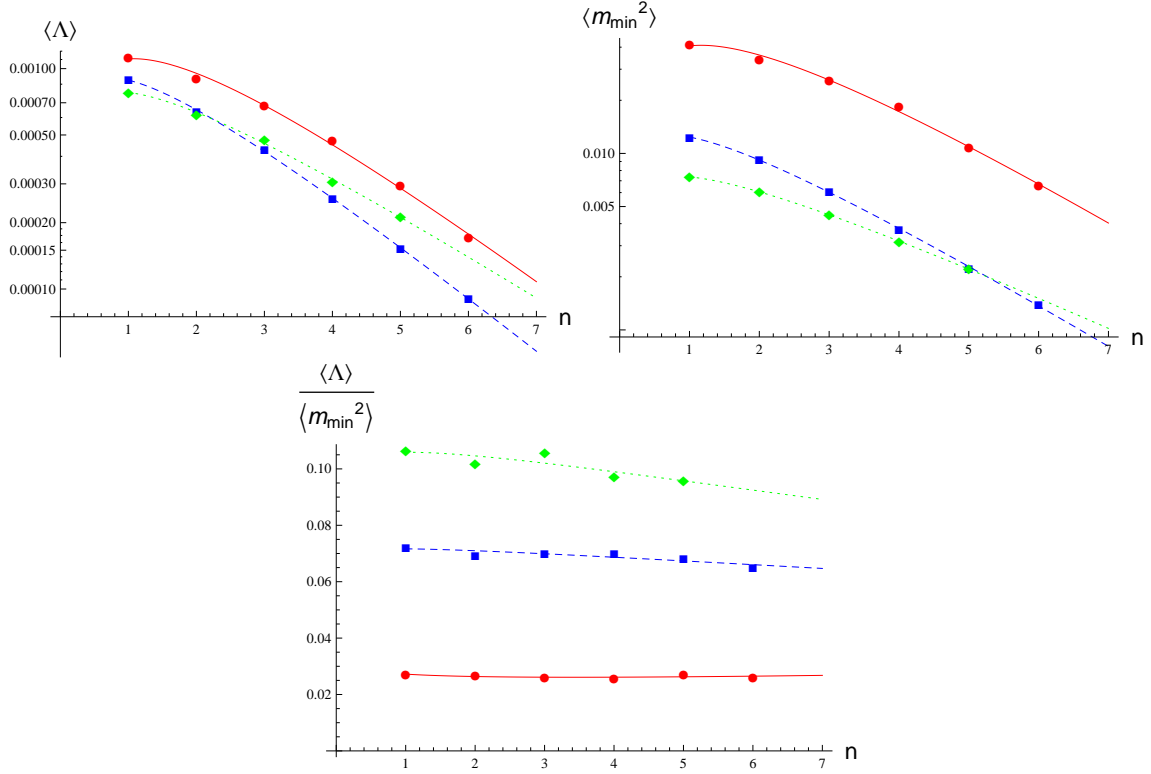


Figure 12: The expectation values where the distribution $P(W_0)$ has a $(n-1)$ th power of logarithmic divergence at $W_0 = 0$, at $N_K = 1$ (red, line, circle), $N_K = 2$ (blue, dashed, square), and $N_K = 3$ (green, dotted, diamond). Each expectation value is suppressed exponentially, though the exponential suppression at $N_K = 1$ is most significant in $\langle \Lambda \rangle$. Note that the first two plots are given as log-plots.

curves for $\langle \Lambda \rangle$ are

$$\begin{aligned}\langle \Lambda \rangle_{N_K=1} &= 0.00201 n^{0.644} e^{-0.597n}, \\ \langle \Lambda \rangle_{N_K=2} &= 0.00164 n^{0.442} e^{-0.616n}, \\ \langle \Lambda \rangle_{N_K=3} &= 0.00127 n^{0.409} e^{-0.491n}.\end{aligned}\tag{4.12}$$

When we compare the coefficients of exponent, which is important for larger n , we see that the effect of the suppression is most significant around $N_K = 2$ though the increase of n seems to work to make the cosmological constant smaller generically.

On the other hand, the expectation value of minimal eigenvalue of the mass matrix are estimated by

$$\begin{aligned}\langle m_{\min}^2 \rangle_{N_K=1} &= 0.0755 n^{0.722} e^{-0.620n}, \\ \langle m_{\min}^2 \rangle_{N_K=2} &= 0.0224 n^{0.422} e^{-0.592n}, \\ \langle m_{\min}^2 \rangle_{N_K=3} &= 0.0115 n^{0.364} e^{-0.448n}.\end{aligned}\tag{4.13}$$

We now see that the coefficients in exponent is quite similar to that of the one for $\langle \Lambda \rangle$. Since we have the W_0 dependence in the coefficient of the potential (4.5) and this coefficient is the

common part between potential and mass matrix, the similar suppression is expected even in the eigenvalue of mass matrix (see also the last plot in Figure 12).

Together with the estimated functions above, now we discuss about the cosmological moduli problem. When we estimate the values $\Lambda \sim 10^{-122}$, $m_{\min}^2 \sim 10^{-30}$ with the fitted functions above, we get the numbers:

N_K	1	2	3
$\langle \Lambda \rangle \sim 10^{-122}$	$n \sim 467$	$n \sim 450$	$n \sim 564$
$\langle m_{\min}^2 \rangle \sim 10^{-30}$	$n \sim 113$	$n \sim 113$	$n \sim 148$

(4.14)

The estimated n for the lower bound of moduli mass is always smaller than that for Λ . Therefore we still encounter the cosmological moduli problem.

4.3 Sharply peaked $P(W_0)$ and $P(A_i)$

In previous subsection, we considered sharply peaked $P(W_0)$ but uniform distribution for A_i . Here we consider the situation where both $P(W_0)$ and $P(A_i)$ are sharply peaked. In this setup, the probability distribution functions of the parameters are given by

$$\begin{aligned}
 P(W_0) &= \frac{1}{15(n-1)!} \left(\ln \frac{15}{|W_0|} \right)^{n-1}, \quad -15 \leq W_0 \leq 0, \\
 P(A_i) &= \frac{1}{(n-1)!} \left(\ln \frac{1}{A_i} \right)^{n-1}, \quad 0 \leq A_i \leq 1.
 \end{aligned}
 \tag{4.15}$$

In the numerical calculation, we can get a result even at $n = 15$ in this setup. This is probably related to the preference of small values of $B_i = A_i/A_1$ to stabilize the model at positive Λ . Now since the distribution of A_i prefers smaller values, the resultant B_i are also likely smaller than that in case of uniform distribution.

The plots for the expectation values are given in Figure 13. The estimated functions for $\langle \Lambda \rangle$ here are given by

$$\begin{aligned}
 \langle \Lambda \rangle_{N_K=1} &= 0.00468 n^{0.0803} e^{-1.40n}, \\
 \langle \Lambda \rangle_{N_K=2} &= 0.00370 n^{0.974} e^{-1.49n}, \\
 \langle \Lambda \rangle_{N_K=3} &= 0.00340 n^{1.48} e^{-1.55n}.
 \end{aligned}
 \tag{4.16}$$

It is interesting that each coefficient of the exponent is below $-2 \ln 2 \sim -1.39$. Since the coefficient appearing in (4.5) is given as a product of $A_1 W_0$, we may naively expect an exponential suppression of the form $e^{-2n \ln 2}$.

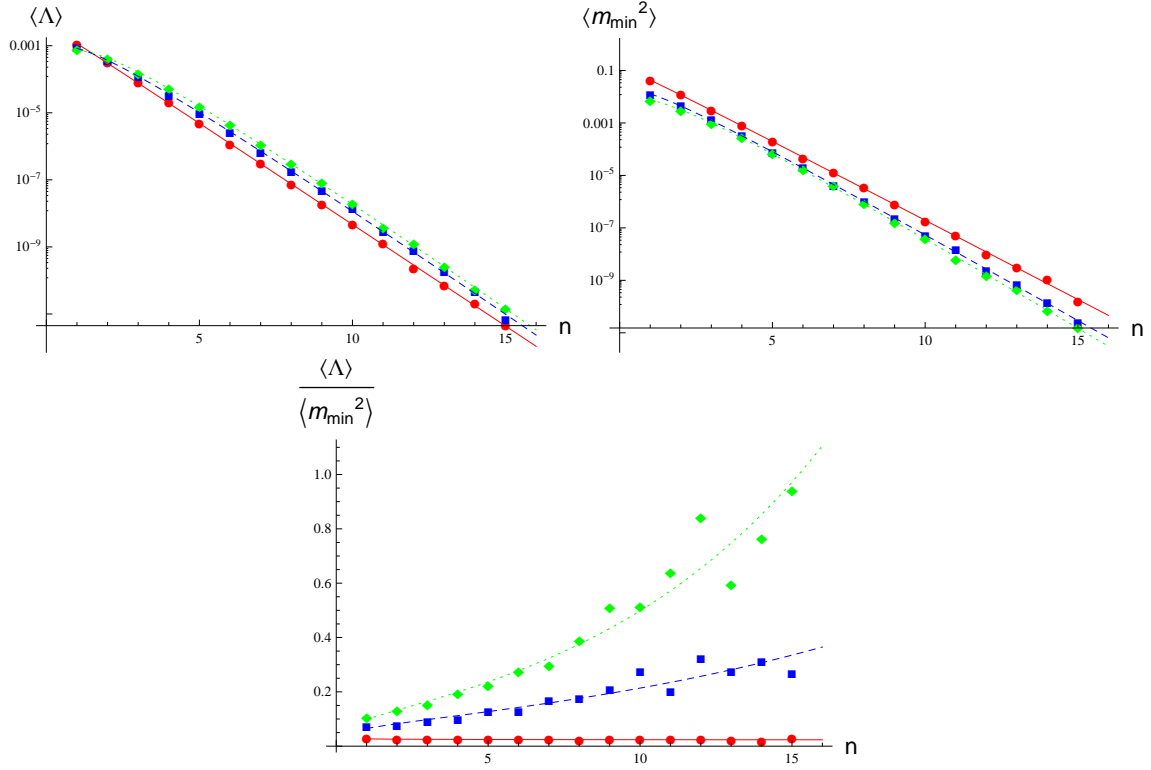


Figure 13: The expectation values with peaked distributions $P(W_0)$ and $P(A_i)$ for the parameters W_0, A_i , with $(n - 1)$ th power of logarithmic divergence at $W_0 = 0$ and $A_i = 0$ respectively. The expectation values are given for $N_K = 1$ (red, line, circle), $N_K = 2$ (blue, dashed, square), and $N_K = 3$ (green, dotted, diamond). Each expectation value is suppressed exponentially, though the exponential suppression at $N_K = 1$ is most significant in $\langle \Lambda \rangle$. Notice that the first two plots are given as log-plots.

The estimated functions for the lowest eigenvalue of mass matrix become

$$\begin{aligned}
 \langle m_{\min}^2 \rangle_{N_K=1} &= 0.175 n^{0.139} e^{-1.40n}, \\
 \langle m_{\min}^2 \rangle_{N_K=2} &= 0.0609 n^{0.732} e^{-1.56n}, \\
 \langle m_{\min}^2 \rangle_{N_K=3} &= 0.0387 n^{1.21} e^{-1.66n}.
 \end{aligned} \tag{4.17}$$

Again, each coefficient of the exponent is below $-2 \ln 2 \sim -1.39$. The non-trivial complicated moduli couplings push the expectation value down further in addition to the suppression by the coefficient. But here, as in the second plot of Figure 13, the expectation value at larger N_K with fixed n always stays at lower value, meaning that the off-diagonal components in the Hessian tends to push the lowest eigenvalue further down as the rank N_K of the Hessian increases. This effect tends to push up the ratio $\langle \Lambda \rangle / \langle m_{\min}^2 \rangle$.

Now we are ready to consider the cosmological moduli problem.

N_K	1	2	3
$\langle \Lambda \rangle \sim 10^{-122}$	$n \sim 197$	$n \sim 188$	$n \sim 182$
$\langle m_{\min}^2 \rangle \sim 10^{-30}$	$n \sim 48$	$n \sim 44$	$n \sim 42$

(4.18)

We see that the required number of n for the lower bound of mass is always smaller than that for the cosmological constant Λ ; therefore we cannot avoid the cosmological moduli problem.

If we compare the result here with the one in previous subsection (4.14), we see that the required n here is much smaller. This is nothing but a benefit of the additional peakiness in A_i , which is considered to come from the effect of multiple moduli stabilization in the complex structure sector. Although so far we have considered up to $N_K = 3$ in this subsection just for simplicity, it is quite possible that we can explain *at least* the small value of Λ naturally in terms of the variety of string landscape. But we also need to handle the cosmological moduli problem simultaneously in some way, which would be quite ubiquitous when we consider multiple moduli space because the eigenvalues repulsion gets more serious in the higher rank mass matrix.

5 Discussions and Remarks

When there is no preference for a small cosmological constant Λ , extreme fine-tuning is necessary to end up with an exponentially small Λ , when the Planck mass M_P is the only scale in the model. Here we show that simple properties of probability theory can lead to a vanishingly small Λ in some stringy scenarios. In particular, the peaking of the probability distribution $P(\Lambda)$ at $\Lambda = 0$ is quite robust. Admittedly, the particular model we study is chosen more for its solvability than for its phenomenological properties. Nevertheless, it is a model that have been extensively studied in the literature and is non-trivial enough to present some interesting features to serve our specific purpose. This possible stringy mechanism for the preference of an exponentially small Λ should be further explored in more realistic stringy scenarios.

In this paper, we consider the simplest model for the complex structure moduli stabilization, in which we only have linear terms of the complex structure moduli U_i in the superpotential W_0 . We can expect more peaked distributions in w_0 if there are cross couplings among U_i in the superpotential. Actually, such cross couplings are quite ubiquitous even in toroidal orientifolds [15]. Therefore it would be important to investigate the probability distributions $P(w_0)$ and $P(\Lambda)$ in the more realistic models to see whether and under what conditions Λ will be naturally vanishingly small. We are encouraged by a preliminary investigation where the peaking behavior of $P(w_0)$ seems to strengthen when quadratic terms of complex structure moduli are introduced into the superpotential. Obviously a more detailed study is required to get a full picture of the distribution of Λ .

In this paper, we assume all parameters are physical parameters that include radiative corrections. In this sense, we are calculating $P(\Lambda)$ for the physical Λ . We are interested in the situation that the corrections are small compared to the original inputs and therefore can be effectively absorbed in the parameters assigned in the model, which we randomize. If we let all the parameters in the model be bare parameters, then the calculated $P(\Lambda)$ is obviously for the bare Λ . In general, when the parameters are randomized, the ranges and distributions of the bare parameters and that of the physical parameters will be different. Since we have only a vague notion of their ranges and distributions, it is important to know when their ranges and distributions will make a difference in the resulting physics. As we believe, the peaking behavior of $P(w_0)$ and $P(\Lambda)$ are quite generic for reasonable ranges and distributions, while $\langle |\Lambda| \rangle$ is more sensitive to the details.

Even if the radiative and other corrections contribute significantly to the potential, we expect that the peaking behavior is still there since the correction terms will bring in non-trivial moduli dependence and the resulting correlation most likely strengthens the peaking behavior in general. It is interesting to see if how the peaking behavior is affected by the presence of the other types of α' and string loop corrections. Also the backreaction of the α' -correction and non-perturbative terms generating the potential for Kähler moduli would be important for complex moduli sector.

Recently it is argued that the D7 tadpole cancellation condition [30] of the system and the holomorphicity of D7-branes in flux compactification restricts the maximal rank of gauge group on D7-branes [31, 32], which is a candidate to derive non-perturbative terms as a result of the gaugino condensation. The explicit solution for dS space was obtained with $\mathbb{C}P_{1,1,1,6,9}^4$ even in the presence of the constraint for a_i [32]. Although we have analyzed statistical behavior only by randomizing W_0, A_i with the other parameters fixed just for simplicity in this paper, it would be interesting to see the effect by randomizing the parameter a_i within the known restrictions/constraints.

We discuss the mass of the lightest modulus. Its very small mass may pose the cosmological moduli problem. This problem may be ameliorated in some multi-field inflationary scenarios [33–35] based on [36]. We also know that radiative correction to the cosmological mass squared goes like M_{SUSY}^2 where M_{SUSY} is the SUSY breaking scale, so the cosmological moduli problem may not be as serious as one expects. In any case, a better understanding of this problem is important if we like to take this stringy mechanism for a vanishingly small Λ seriously. If we impose the present cosmological moduli constraint, we can bring Λ down only a limited number of orders of magnitude. It is entirely possible that the stringy mechanism discussed in this paper provides only a partial solution to the Λ problem.

Acknowledgment

We have benefited from discussions with Lam Hui, Liam McAllister, Fernando Quevedo, Markus Rummel, Gary Shiu, Zheng Sun, Alexander Westphal, and Tsutomu Yanagida. YS is grateful to Isaac Newton Institute for Mathematical Sciences and the organizers of “String Phenomenology 2012”, and also the organizers of “The 3rd UTQuest workshop ExDiP 2012 on Superstring and Cosmophysics” for their great hospitality, where some of the results were presented.

A Some toy models

To get some feeling on the peaking property for the probability distribution $P(\Lambda)$ of Λ , consider the single field polynomial model. At least three terms with different powers are required to achieve the metastable vacua with a positive Λ [37–40]. Since we are interested in only the meta-stable solution, we may consider a model of a simple minimal form:

$$V(\phi) = a\phi - \frac{b}{2}\phi^2 + \frac{c}{3!}\phi^3 \quad (\text{A.1})$$

where all parameters are positively defined for simplicity, and have the scale M_P^4 . Now, we impose the stability $\partial_\phi^2 V|_{\min} > 0$ at the extremal points given by $\partial_\phi V = 0$. These conditions imply

$$\Delta \equiv \sqrt{b^2 - 2ac} > 0, \quad \phi_{\min} = \frac{b + \Delta}{c}. \quad (\text{A.2})$$

Plugging back to the potential, we get

$$\Lambda \equiv V_{\min} = \frac{(b + \Delta)^2(b - 2\Delta)}{6c^2}. \quad (\text{A.3})$$

So we see that the sum form (A.1) is converted to the product form (A.3).

If we impose the positivity of the potential $\Lambda \geq 0$, then the parameter region is further restricted by

$$1 < C_p \leq \frac{4}{3}, \quad C_p \equiv \frac{b^2}{2ac}, \quad (\text{A.4})$$

where the lower bound is given by the stability while the upper bound is for the positivity. Whenever we satisfy the region of the combined parameter above, there exists a minimum with positive Λ . Since we are interested in the region with small Λ s, let us further focus on the region around $C_p \sim 4/3$. Then the potential becomes

$$\Lambda \sim \frac{9ab}{8c} \left(\frac{4}{3} - C_p \right). \quad (\text{A.5})$$

Next we analyze the distribution of the approximate minima (A.5). To make the argument simple, we here fix $c = 1$ and take a, b as random parameters obeying uniform distribution

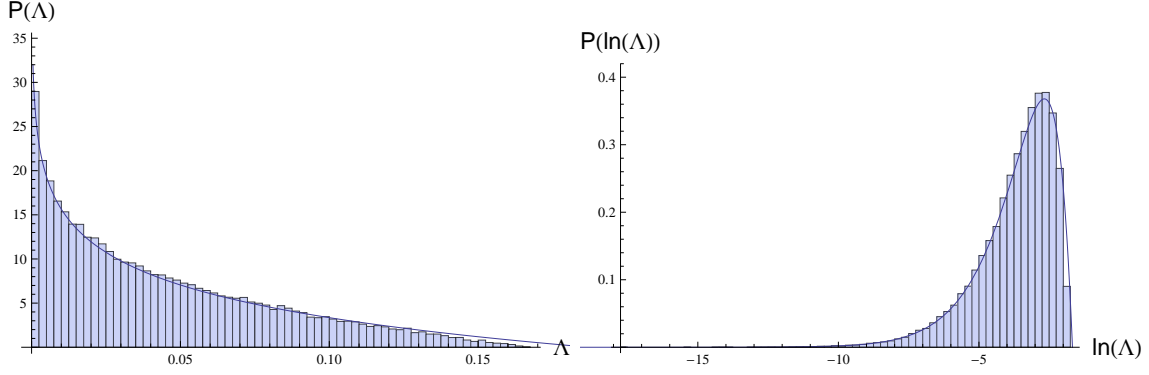


Figure 14: The comparison of the analytical (the curve) and the numerical (the histogram) distributions $P(\Lambda)$ vs Λ (LHS) and $P(\ln \Lambda)$ vs $\ln \Lambda$ (RHS) in the polynomial model (A.1).

within a range $0 \leq a, b \leq 1$. Then the probability distribution function is estimated to be

$$P(\Lambda) = N_0^{-1} \int dC_p \int_0^1 da db \delta\left(\frac{9}{8}ab\left(\frac{4}{3} - C_p\right) - \Lambda\right) \delta\left(\frac{b^2}{2a} - C_p\right), \quad (\text{A.6})$$

where N_0 is the normalization constant. Performing the last two integrals for the two δ -functions, being careful with the integration regions, we get

$$P(\Lambda) = N_0^{-1} \int dC_p \frac{1}{3C_p(4/3 - C_p)}, \quad 1 < C_p \leq \frac{12}{9 + 16\Lambda}. \quad (\text{A.7})$$

The constraint for C_p also suggests $0 \leq \Lambda < 3/16$. The normalization constant N_0 is calculated such that $\int d\Lambda P(\Lambda) = 1$, which gives $N_0 = 1/24$, so

$$P(\Lambda) = \frac{16}{3} \ln \left[\frac{3}{16\Lambda} \right]. \quad (\text{A.8})$$

where $P(\Lambda)$ is divergent at $\Lambda = 0$. This is nothing but the outcome of the product form of the coefficient obtained in (A.5). If we allow the parameter c to have a distribution (even including zero), the divergence at $\Lambda = 0$ is still present (see the argument for ratio distributions, e.g. in [3]). However, $P(\Lambda)$ will have a longer tail at large Λ .

Although we have analyzed the approximate potential (A.5), we can easily check numerically the divergent behavior (A.8) at the minimum (A.3) in the full form of the potential. In Figure 14, the analytical function (A.8) perfectly agrees with the numerical histogram especially at lower values, given uniformly distributed random values for $0 \leq a, b \leq 1$ while fixing $c = 1$.

Next, consider a simple multi-field case,

$$V(\phi_i) = A_i \phi_i + B_{ij} \phi_i \phi_j$$

We see that

$$V_{\min} = -A^T B^{-1} A$$

which is a sum of terms for the multi-field cases. Clearly the B_{ij} coupling alone is not enough for V_{\min} to take the product form. Higher couplings for tighter interactions among the fields are necessary to bring V_{\min} to the product form.

Although we do not have an analytic form for V_{\min} for more complicated $V(\phi)$, it is easy to convince oneself (and check numerically) that a divergent $P(\Lambda)$ at $\Lambda = 0$ for meta-stable V_{\min} is quite typical for V in which all terms are tightly coupled to each other.

For more complicated $V(\phi)$, V_{\min} takes a more complicated form. We are looking for 2 features : (1) whether the probability distribution $P(\Lambda)$ has a peaking (maybe even divergent) behavior at $\Lambda = 0$, and the peakiness becomes more pronounced as the number of fields and their couplings (parameters treated as random variables) increase; and (2) whether the expectation value of the magnitude $\langle \Lambda \rangle$ is dropping exponentially fast as the number of fields increases.

B $P(\Lambda)$ in the single Kähler modulus case

We show here the way to estimate the probability distribution $P(\Lambda)$ in the single Kähler modulus case discussed in section 2.2. Let us define

$$w_1 = -W_0, \quad w_2 = A_1, \quad c = \frac{w_1}{w_2} = \frac{64\sqrt{2}}{27}C. \quad (\text{B.1})$$

and set the value $a_1 = \gamma_1 = \hat{\xi} = 1$. Neglecting the overall coefficient, the model is simplified to be

$$z = w_1 w_2 (c - c_0), \quad c_0 \leq c = \frac{w_1}{w_2} < c_1, \quad (\text{B.2})$$

where $c_0 \sim 12.2$ and $c_1 \sim 13.0$. The cosmological constant is related with this z through the relation $\Lambda = 3z/(2500\sqrt{5})$.

Now the probability distribution of z is determined by

$$P(z) = N_0^{-1} \int_{c_0}^{c_1} dc \int_0^1 dw_1 dw_2 \delta(w_1 w_2 (c - c_0)) \delta\left(\frac{w_1}{w_2} - c\right), \quad (\text{B.3})$$

where N_0 is the normalization constant. Since this is the constrained integrations by two delta functions, the integrated region is further constrained. The last two integrations can be achieved easily and we get

$$P(z) = \begin{cases} N_0^{-1} \int dc \frac{1}{2c(c-c_0)} & \text{for } 0 \leq z \leq c(c-c_0), \quad c \leq 1, \\ N_0^{-1} \int dc \frac{1}{2c(c-c_0)} & \text{for } 0 \leq z \leq \frac{c-c_0}{c}, \quad c \geq 1. \end{cases} \quad (\text{B.4})$$

Since the region of c of interest is $1 < c_0 \leq c < c_1$, we can integrate over c and

$$\begin{aligned} P(z) &= N_0^{-1} \int_{\frac{c_0}{1-z}}^{c_1} dc \frac{1}{2c(c-c_0)} = \frac{c_1}{c_1-c_0} \ln \left[\frac{c_1-c_0}{c_1 z} \right], \\ N_0 &= \int_0^{\frac{c_1-c_0}{c_1}} dz \int_{\frac{c_0}{1-z}}^{c_1} dc \frac{1}{2c(c-c_0)} = \frac{c_1-c_0}{2c_1 c_0}. \end{aligned} \quad (\text{B.5})$$

The probability distribution of Λ can be estimated via the relation $P(\Lambda) d\Lambda = P(z) dz$ by,

$$P(\Lambda) = \frac{2500\sqrt{5}}{3} \frac{c_1}{c_1-c_0} \ln \left[\frac{3}{2500\sqrt{5}} \frac{c_1-c_0}{c_1 \Lambda} \right]. \quad (\text{B.6})$$

which is (2.12).

C Special symmetric case for s and w_0

Some of the manifolds have special symmetries so it is interesting to see the impact of them on the value of s and the probability distribution $P(w_0)$.

Let $r_i = d_i/b_i$ and $r_0 = c_2/c_1$. Let us consider the special situation,

$$r \equiv r_1 = r_2 = \dots = r_i = \dots = r_{h^{2,1}}, \quad (\text{C.1})$$

while $r \neq r_0$. Following from (3.7), all complex structure moduli u_i are equal. Then the solution of (3.10) is given by

$$s = \frac{1}{2rr_0} \left[(h^{2,1} - 1)(r - r_0) \pm \sqrt{(h^{2,1} - 1)^2(r - r_0)^2 + 4rr_0} \right], \quad (\text{C.2})$$

which, for large $h^{2,1}$ yields, for $r > r_0$,

$$s \sim (h^{2,1} - 1) \frac{r - r_0}{rr_0}, \quad \text{or} \quad \frac{1}{(h^{2,1} - 1)(r - r_0)}, \quad (\text{C.3})$$

in which case, r must be close to r_0 and $r_0 > r$ for s to be large and positive. In this case, we now have

$$W_0|_{\min} = \frac{c_1}{h^{2,1}} (1 + sr_0) \left(\frac{1 - sr}{1 + sr} \right). \quad (\text{C.4})$$

It is easy to see that the strong peaking behavior of $P(w_0)$ is absent here.

At the symmetric point, $b_i = d_i$ or $r = r_i = 1$, (C.3) reduces to

$$s \sim (h^{2,1} - 1) \left(\frac{c_1}{c_2} - 1 \right). \quad (\text{C.5})$$

Recall that we like s to be large and positive, say $s \approx 10$, so we need $c_1 > c_2$.

The following picture emerges. As we move towards the symmetric points, the probability distribution $P(w_0)$ loses its peaking behavior at $\Lambda = 0$. This is simply because (the random) parameter space collapses at the symmetric points.

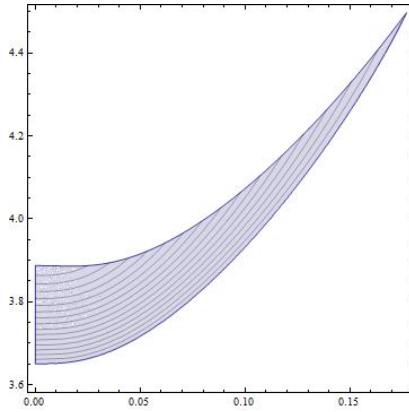


Figure 15: The validity region in $B_2 - C$ plane for meta-stable dS vacua with two moduli. The x -axis is B_2 and the y -axis is C . The contours inside the region describe level lines of \mathcal{U} , not the magnitude of Λ .

D Stabilization in two and three Kähler moduli models

For the analysis of the potential for multi-Kähler moduli in section 4, we elaborate on the stability analysis in the cases of two and three Kähler moduli. Here we just focus on the bracket part of (4.5) since the coefficient part does not touch the stability. For convenience, we further define

$$\mathcal{U} \equiv \frac{2C}{9(x_1^{3/2} - \sum_{j=2} \delta_j x_j^{3/2})^3} - \frac{x_1 e^{-x_1}}{(x_1^{3/2} - \sum_{j=2} \delta_j x_j^{3/2})^2} - \sum_{i=2} \frac{B_i x_i e^{-x_i}}{(x_1^{3/2} - \sum_{j=2} \delta_j x_j^{3/2})^2}. \quad (\text{D.1})$$

D.1 Two Kähler moduli

Let us start with the two moduli case. In the region $\delta_2 \ll 1$, the stabilization of x_1 is little changed from that of the single Kähler case. Therefore the moduli stabilization for x_2 requires small B_2 so the third term in (4.5) is comparable with the other terms proportional to δ_2 . The situation begins to differ from the single Kähler case as δ_2 increases. But since the volume is defined to be positive and we expect the fixed moduli value of x_2 to be comparable with x_1 , δ_2 should not be too large. So hereafter we take $\delta_2 = 1$ just for simplicity. For stability, we need to be careful about the positivity of mass matrix. According to *Sylvester criteria* (see e.g. [41], which is also used in [42]), we consider positivity of $\partial_{x_1}^2 \mathcal{U}$ and the determinant of the 2×2 matrix $\partial_{x_i} \partial_{x_j} \mathcal{U}$, simultaneously with the positivity of the extremal points.

The extremal conditions $\partial_{x_i}\mathcal{U} = 0$ are solved by

$$\begin{aligned}
C &= \frac{e^{-x_1}}{\sqrt{x_1}(x_2 - 1)} \\
&\times \left[(2x_1^3 + x_1^4)(x_2 - 1) - x_1^{3/2}x_2^{3/2}(x_2 - 4) + (x_1x_2^3 - x_2^3)(x_2 + 2) - x_1^{5/2}x_2^{3/2}(2x_2 + 1) \right], \\
B_2 &= \frac{e^{-x_1+x_2}(x_1 - 1)}{(1 - x_2)} \sqrt{\frac{x_2}{x_1}}.
\end{aligned} \tag{D.2}$$

If we take $x_2 \rightarrow 0$, the conditions recover that for the single Kähler case. Together with the positive mass squared conditions above, Figure 15 shows the allowed parameters region with respect to C, B_2 for meta-stable dS vacua. In the system above, the positivity constraint of the determinant controls the upper bound of the parameter region in Figure 15, while the lower bound is given by the positivity constraint $\mathcal{U} > 0$. The contours inside the region describe level lines of \mathcal{U} , not the magnitude of Λ . On the other hand, $\Lambda = 0$ at the top boundary curve, and Λ increases as we move down away from this boundary. The numerical values of the parameters in the region are roughly given by

$$3.650 \lesssim C \lesssim 4.498, \quad 0 < B_2 \lesssim 0.1769. \tag{D.3}$$

For instance, the lower bound of the parameters requires the potential minimum at

$$x_1 = 2.5, \quad x_2 = 0, \tag{D.4}$$

while the upper bound of the parameters suggests the minimum at around

$$x_1 \sim 3.881, \quad x_2 \sim 0.7085. \tag{D.5}$$

Note that the value of \mathcal{U} increases gradually with C , similar to the single Kähler modulus case.

Note that the validity range of the C parameter is different from the one obtained for single Kähler moduli. The result for single Kähler modulus case is [7]

$$3.650 \lesssim C \lesssim 3.887, \quad B_2 = 0. \tag{D.6}$$

Therefore we see that the additional modulus dependence alleviates the constraint for C parameter, but still restricts B_2 small. We may understand the smallness of B_2 as a consequence of the positivity of the volume \mathcal{V} defined in (4.1). The required smallness of $\sum_{i=2} \gamma_i t_i / \gamma_1 t_1$ affects the combinations A_i/A_1 to stabilize the potential in entire Kähler moduli space. Therefore A_i/A_1 cannot be large and are about the same order of x_i/x_1 (or the combination of $\delta_i x_i/x$) at the dS minima.

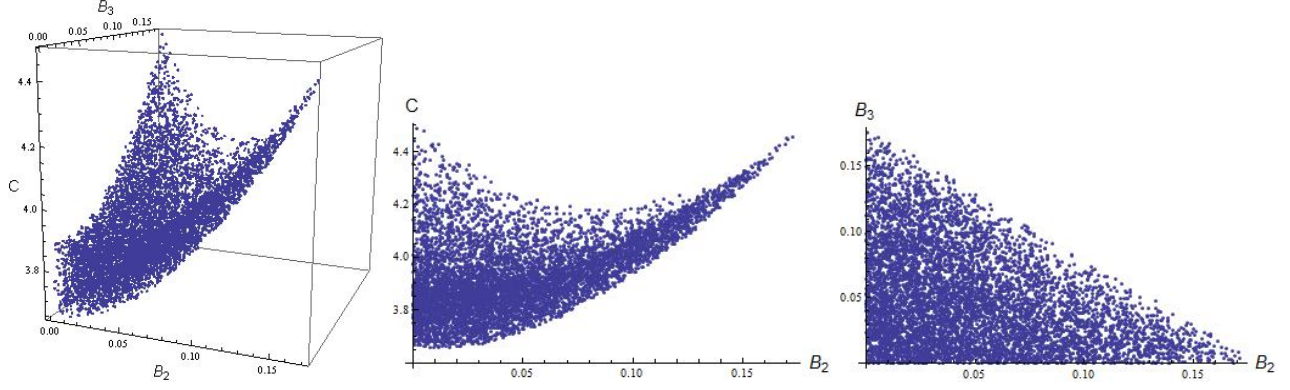


Figure 16: The parameter region in the $B_2 - C - B_3$ plot shows the stable minima at positive Λ with three moduli. The last two figures display the data on a projected plane.

D.2 Three Kähler moduli

Now let us proceed to the model with three Kähler moduli case. Since it is difficult to draw figures with continuous surfaces, here we use the numerical data given random values for parameters assigned to the model. Similar to the two moduli case, we set $\delta_2 = \delta_3 = 1$ just for simplicity.

Given the values for parameters C, B_2, B_3 obeying uniform distribution, we get the region of parameter sets which satisfy the stability condition at positive Λ , shown in Figure 16. All points here satisfy the stability constraint at extremal points with $\Lambda \geq 0$. We see that the stable parameter region for three moduli case includes the stable region for two moduli case as a boundary. The restricted ranges for the parameters are given by

$$3.650 \lesssim C \lesssim 4.498, \quad 0 < B_2 \lesssim 0.1769, \quad 0 < B_3 \lesssim 0.1769. \quad (\text{D.7})$$

The parameters are correlated so they are further constrained.

D.3 Checking the validity of the approximate potential

So far we have seen what happens in the approximate potential (D.1). Here let us compare the resultant parameter space with that of the full potential (4.1). The full potential is no longer written down in terms of the combined parameters (4.4). Therefore we give values for W_0, A_i and set $a_i = \gamma_i = \hat{\xi} = 1$ for simplicity, and solve for moduli fields t_i .

The full potential for two Kähler moduli suggests the stable parameter region for C, B_2 as in LHS of Figure 17, where

$$3.95 \lesssim C \lesssim 4.87, \quad 0 < B_2 \lesssim 0.193. \quad (\text{D.8})$$

Although the boundary values for parameter region are changed a little from the approximate

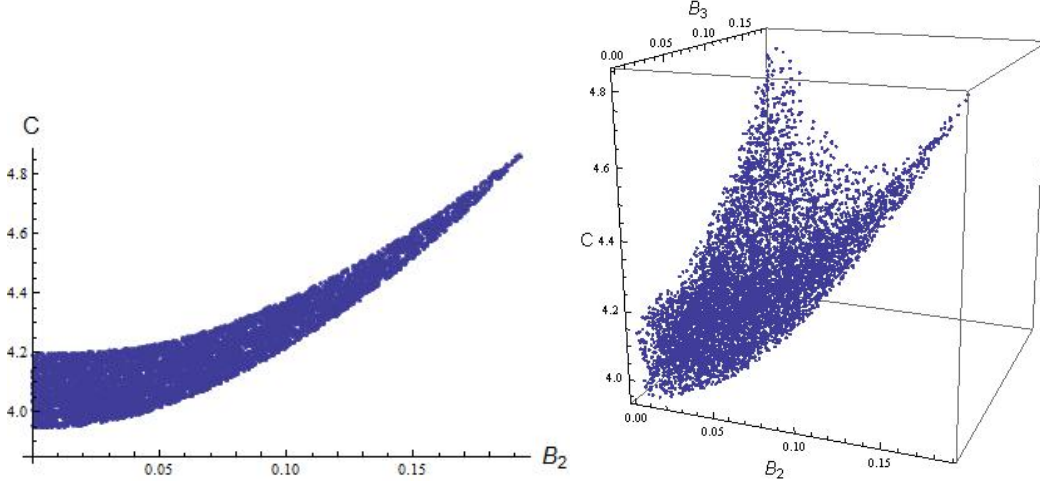


Figure 17: The stable parameter region for dS vacua in the full potential (4.1) for the two and three moduli case.

ones (D.3) for the approximate potential (4.5), the essential feature is unchanged, including the shape of the region which is crucial for the distribution of Λ .

In the three moduli model, the full potential also suggests the similar parameter region for stability to that for the approximate potential. The stability condition at positive Λ is satisfied if the parameters are within the region in RHS of Figure 17, suggesting roughly

$$3.95 \lesssim C \lesssim 4.87, \quad 0 < B_2 \lesssim 0.193, \quad 0 < B_3 \lesssim 0.193. \quad (\text{D.9})$$

Again, though the values are changed a little from (D.7), the shape of stable region is the same as before.

From the examples of the analysis of the full potential above, we see the basic agreements between the approximate potential and the full potential, at least for the distribution analysis of small Λ . This approximation is quite helpful if we like to go beyond three Kähler moduli. Thus, as in single modulus case in section 2.2, we may use the approximate potential (4.5) to understand the statistical properties of the potential (4.1) for the general multi-Kähler moduli cases studied in section 4.

References

- [1] E. Komatsu *et al.*, “Seven-Year Wilkinson Microwave Anisotropy Probe (WMAP) Observations: Cosmological Interpretation,” *Astrophys.J.Suppl.* **192** (Jan., 2011) 18, 1001.4538.

- [2] R. Bousso and J. Polchinski, “Quantization of four form fluxes and dynamical neutralization of the cosmological constant,” *JHEP* **0006** (2000) 006, [arXiv:hep-th/0004134](#) [[hep-th](#)].
- [3] Y. Sumitomo and S.-H. H. Tye, “A Stringy Mechanism for A Small Cosmological Constant,” *JCAP* **1208** (2012) 032, [arXiv:1204.5177](#) [[hep-th](#)].
- [4] M. R. Douglas and S. Kachru, “Flux compactification,” *Rev.Mod.Phys.* **79** (2007) 733–796, [arXiv:hep-th/0610102](#).
- [5] V. Balasubramanian and P. Berglund, “Stringy corrections to Kahler potentials, SUSY breaking, and the cosmological constant problem,” *JHEP* **0411** (2004) 085, [arXiv:hep-th/0408054](#) [[hep-th](#)].
- [6] A. Westphal, “de Sitter string vacua from Kahler uplifting,” *JHEP* **0703** (2007) 102, [arXiv:hep-th/0611332](#).
- [7] M. Rummel and A. Westphal, “A sufficient condition for de Sitter vacua in type IIB string theory,” *JHEP* **1201** (2012) 020, [arXiv:1107.2115](#) [[hep-th](#)].
- [8] S. de Alwis and K. Givens, “Physical Vacua in IIB Compactifications with a Single Kaehler Modulus,” *JHEP* **1110** (2011) 109, [arXiv:1106.0759](#) [[hep-th](#)].
- [9] V. Balasubramanian, P. Berglund, J. P. Conlon, and F. Quevedo, “Systematics of moduli stabilisation in Calabi-Yau flux compactifications,” *JHEP* **0503** (2005) 007, [hep-th/0502058](#).
- [10] S. Kachru, R. Kallosh, A. D. Linde, and S. P. Trivedi, “De Sitter vacua in string theory,” *Phys.Rev.* **D68** (2003) 046005, [arXiv:hep-th/0301240](#).
- [11] K. Becker, M. Becker, M. Haack, and J. Louis, “Supersymmetry breaking and alpha-prime corrections to flux induced potentials,” *JHEP* **0206** (2002) 060, [hep-th/0204254](#).
- [12] J. P. Conlon, F. Quevedo, and K. Suruliz, “Large-volume flux compactifications: Moduli spectrum and D3/D7 soft supersymmetry breaking,” *JHEP* **0508** (2005) 007, [arXiv:hep-th/0505076](#) [[hep-th](#)].
- [13] M. Cicoli, J. P. Conlon, and F. Quevedo, “General Analysis of LARGE Volume Scenarios with String Loop Moduli Stabilisation,” *JHEP* **0810** (2008) 105, [arXiv:0805.1029](#) [[hep-th](#)].
- [14] J. Gray, Y.-H. He, V. Jejjala, B. Jurke, B. D. Nelson, *et al.*, “Calabi-Yau Manifolds with Large Volume Vacua,” [arXiv:1207.5801](#) [[hep-th](#)].
- [15] D. Lust, S. Reffert, W. Schulgin, and S. Stieberger, “Moduli stabilization in type IIB orientifolds (I): Orbifold limits,” *Nucl.Phys.* **B766** (2007) 68–149, [arXiv:hep-th/0506090](#) [[hep-th](#)].

- [16] A. Aazami and R. Easther, “Cosmology from random multifield potentials,” *JCAP* **0603** (2006) 013, [hep-th/0512050](#).
- [17] D. S. Dean and S. N. Majumdar, “Large deviations of extreme eigenvalues of random matrices,” *Phys.Rev.Lett.* **97** (2006) 160201, [cond-mat/0609651](#).
- [18] D. S. Dean and S. N. Majumdar, “Extreme value statistics of eigenvalues of gaussian random matrices,” *Phys. Rev. E*, **77**, (Jan., 2008) 041108, [0801.1730](#).
- [19] G. Borot, B. Eynard, S. Majumdar, and C. Nadal, “Large deviations of the maximal eigenvalue of random matrices,” *J.Stat.Mech.* **1111** (2011) P11024, [arXiv:1009.1945 \[math-ph\]](#).
- [20] X. Chen, G. Shiu, Y. Sumitomo, and S.-H. H. Tye, “A Global View on The Search for de-Sitter Vacua in (type IIA) String Theory,” *JHEP* **1204** (2012) 026, [arXiv:1112.3338 \[hep-th\]](#).
- [21] T. C. Bachlechner, D. Marsh, L. McAllister, and T. Wrase, “Supersymmetric Vacua in Random Supergravity,” [arXiv:1207.2763 \[hep-th\]](#).
- [22] G. Coughlan, W. Fischler, E. W. Kolb, S. Raby, and G. G. Ross, “Cosmological Problems for the Polonyi Potential,” *Phys.Lett.* **B131** (1983) 59.
- [23] T. Banks, D. B. Kaplan, and A. E. Nelson, “Cosmological implications of dynamical supersymmetry breaking,” *Phys.Rev.* **D49** (1994) 779–787, [hep-ph/9308292](#).
- [24] B. de Carlos, J. Casas, F. Quevedo, and E. Roulet, “Model independent properties and cosmological implications of the dilaton and moduli sectors of 4-d strings,” *Phys.Lett.* **B318** (1993) 447–456, [hep-ph/9308325](#).
- [25] F. Denef and M. R. Douglas, “Distributions of flux vacua,” *JHEP* **0405** (2004) 072, [arXiv:hep-th/0404116](#).
- [26] M. Cicoli, J. P. Conlon, and F. Quevedo, “Systematics of String Loop Corrections in Type IIB Calabi-Yau Flux Compactifications,” *JHEP* **0801** (Aug., 2008) 052, [0708.1873](#).
- [27] M. Berg, M. Haack, and E. Pajer, “Jumping Through Loops: On Soft Terms from Large Volume Compactifications,” *JHEP* **0709** (2007) 031, [arXiv:0704.0737 \[hep-th\]](#).
- [28] M. Kawasaki, K. Kohri, and N. Sugiyama, “Cosmological constraints on late time entropy production,” *Phys.Rev.Lett.* **82** (1999) 4168, [arXiv:astro-ph/9811437 \[astro-ph\]](#).
- [29] M. Kawasaki, K. Kohri, and N. Sugiyama, “MeV scale reheating temperature and thermalization of neutrino background,” *Phys.Rev.* **D62** (2000) 023506, [arXiv:astro-ph/0002127 \[astro-ph\]](#).
- [30] A. Collinucci, F. Denef, and M. Esole, “D-brane Deconstructions in IIB Orientifolds,” *JHEP* **0902** (2009) 005, [arXiv:0805.1573 \[hep-th\]](#).

- [31] M. Cicoli, C. Mayrhofer, and R. Valandro, “Moduli Stabilisation for Chiral Global Models,” *JHEP* **1202** (2012) 062, [arXiv:1110.3333 \[hep-th\]](#).
- [32] J. Louis, M. Rummel, R. Valandro, and A. Westphal, “Building an explicit de Sitter,” [arXiv:1208.3208 \[hep-th\]](#).
- [33] F. Takahashi and T. T. Yanagida, “Strong dynamics at the Planck scale as a solution to the cosmological moduli problem,” *JHEP* **1101** (2011) 139, [arXiv:1012.3227 \[hep-ph\]](#).
- [34] F. Takahashi and T. T. Yanagida, “Why have supersymmetric particles not been observed?,” *Phys.Lett.* **B698** (2011) 408–410, [arXiv:1101.0867 \[hep-ph\]](#).
- [35] R. Kallosh, A. Linde, K. A. Olive, and T. Rube, “Chaotic inflation and supersymmetry breaking,” *Phys.Rev.* **D84** (2011) 083519, [arXiv:1106.6025 \[hep-th\]](#).
- [36] A. D. Linde, “Relaxing the cosmological moduli problem,” *Phys.Rev.* **D53** (1996) 4129–4132, [hep-th/9601083](#).
- [37] A. Maloney, E. Silverstein, and A. Strominger, “De Sitter space in noncritical string theory,” [arXiv:hep-th/0205316 \[hep-th\]](#).
- [38] E. Silverstein, “TASI / PiTP / ISS lectures on moduli and microphysics,” [arXiv:hep-th/0405068 \[hep-th\]](#).
- [39] E. Silverstein, “Simple de Sitter Solutions,” *Phys.Rev.* **D77** (2008) 106006, [arXiv:0712.1196 \[hep-th\]](#).
- [40] S. S. Haque, G. Shiu, B. Underwood, and T. Van Riet, “Minimal simple de Sitter solutions,” *Phys.Rev.* **D79** (2009) 086005, [arXiv:0810.5328 \[hep-th\]](#).
- [41] G. T. Gilbert, “Positive definite matrices and sylvester’s criterion,” *The American Mathematical Monthly* **98** (1991) no. 1, pp. 44–46.
<http://www.jstor.org/stable/2324036>.
- [42] G. Shiu and Y. Sumitomo, “Stability Constraints on Classical de Sitter Vacua,” *JHEP* **1109** (2011) 052, [arXiv:1107.2925 \[hep-th\]](#).